Article

Cell Reports

Potentiating dendritic cell immunotherapy by interrupting the Semaphorin 4D-induced immune-suppressive barrier

Graphical abstract

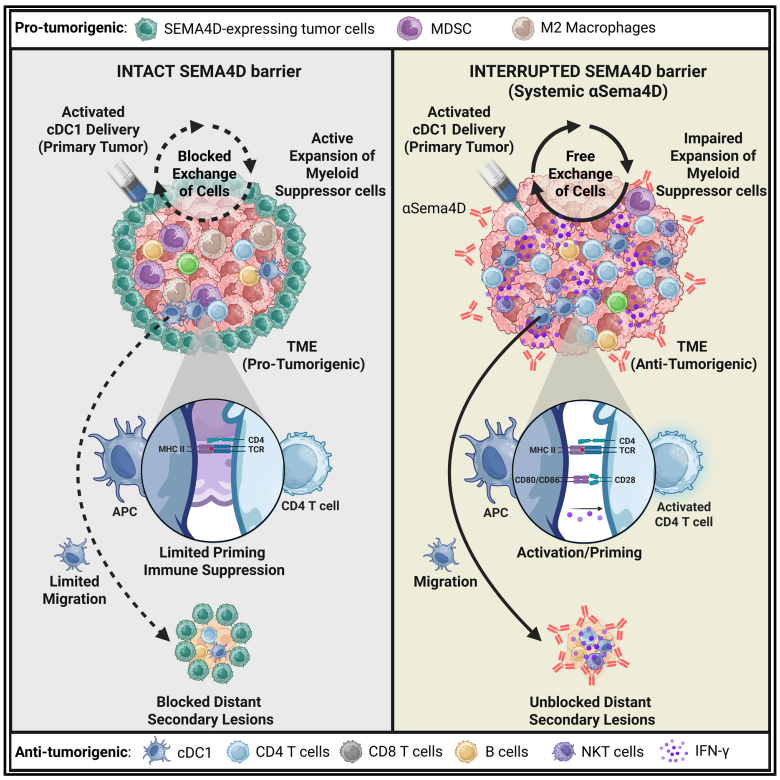

Highlights

- SEMA4D blockade enhances cDC1-mediated immunity in HER2^{+} breast cancer
- Combination therapy increases effector T cell infiltration and reduces MDSCs
- Dual targeting eradicates local and distant tumors via systemic immune activation
- Strategy shows favorable safety and potential for SEMA4D-high malignancies

Authors

Saurabh K. Garg, Colin Snyder, Ganesan Ramamoorthi, ..., Maurice Zauderer, Gary K. Koski, Brian J. Czerniecki

Correspondence

brian.czerniecki@moffitt.org

In brief

Garg et al. report that blocking the molecule SEMA4D strengthens immune responses against HER2-positive breast cancer. When paired with specialized dendritic cells, this approach boosts anti-tumor immune activity, reduces suppressive cells, and enables clearance of both local and distant tumors. Their findings support a promising and well-tolerated immunotherapy strategy.

Garg et al., 2026, Cell Reports *45*, 117050
March 24, 2026 © 2026 The Author(s). Published by Elsevier Inc.
https://doi.org/10.1016/j.celrep.2026.117050

CellPress

Cell Reports

CellPress
OPEN ACCESS

Article

Potentiating dendritic cell immunotherapy by interrupting the Semaphorin 4D-induced immune-suppressive barrier

Saurabh K. Garg,[1,10] Colin Snyder,[1,10] Ganesan Ramamoorthi,[1,10] Krithika N. Kodumudi,[1] Elizabeth E. Evans,[2] Vincent Lok,[3] Holm Bussler,[2] Jonathan V. Nguyen,[4] Jiqiang Yao,[5] Amrita Basu,[1,9] Namrata Gautam,[1] Julio A. Vazquez Martinez,[6] Darwin C. Chang,[6] Amy L. Aldrich,[1] Doris Wiener,[1] Paulo C. Rodriguez,[6] Maurice Zauderer,[2] Gary K. Koski,[7] and Brian J. Czerniecki[8,11,*]

[1]Clinical Science Division, H. Lee Moffitt Cancer Center and Research Institute, Tampa, FL 33612, USA
[2]Vaccinex, Inc., Rochester, NY 14620, USA
[3]Morsani College of Medicine, University of South Florida, Tampa, FL 33612, USA
[4]Advanced Analytical and Digital Laboratory, H. Lee Moffitt Cancer Center and Research Institute, Tampa, FL 33612, USA
[5]Department of Bioinformatics and Biostatistics, H. Lee Moffitt Cancer Center and Research Institute, Tampa, FL 33612, USA
[6]Department of Immunology, H. Lee Moffitt Cancer Center and Research Institute, Tampa, FL 33612, USA
[7]Department of Biological Sciences, Kent State University, Kent, OH 44240, USA
[8]Department of Breast Oncology, H. Lee Moffitt Cancer Center and Research Institute, Tampa, FL 33612, USA
[9]Present address: Department of Pathology and Laboratory Medicine, Nationwide Children's Hospital, Columbus, OH 43205, USA
[10]These authors contributed equally
[11]Lead contact
*Correspondence: brian.czerniecki@moffitt.org
https://doi.org/10.1016/j.celrep.2026.117050

SUMMARY

Immune suppression within the tumor microenvironment (TME) remains a significant barrier to effective cancer immunotherapy, including dendritic cell (DC)-based approaches. We address this by targeting Semaphorin 4D (SEMA4D), a pro-tumorigenic mediator expressed by leading-edge tumor cells and host immune cells, particularly in HER2-positive (HER2^{pos}) breast cancer (BC). Antibody blockade of SEMA4D enhances the efficacy of adoptively transferred tumor-specific conventional type 1 DCs (cDC1s) across multiple HER2^{pos} BC models. Tumor-cell-specific ablation of SEMA4D activity amplifies cDC1-driven anti-tumor immunity, highlighting its role in immune evasion. SEMA4D blockade synergizes with cDC1s to increase CD4^{+} Th1 and other effector cell infiltration into the TME, along with reciprocal elimination of myeloid-derived suppressor cells, fostering robust systemic immune responses that eradicated both local and distant tumors. Given its favorable safety profile, this strategy represents a promising immunotherapy for malignancies, including HER2^{pos} BC that express high levels of SEMA4D in both tumor and stromal compartments.

INTRODUCTION

Dendritic cells (DCs) are potent antigen-presenting cells that shape innate and adaptive immune responses.[1] DC-based immunotherapy has traditionally been evaluated as a tumor-antigen-loaded vaccine injected subcutaneously or directly into lymph nodes, aimed at developing adaptive memory T cell responses.[2–5] With this traditional vaccine paradigm, our group found that conventional type 1 DCs (cDC1s) provide only limited efficacy in patients with early ductal carcinoma *in situ*.[6–8] However, in subsequent murine models, we discovered that switching the delivery route to direct intratumoral (i.t.) administration significantly improves the efficacy of cDC1 immunotherapies to provide enhanced anti-tumor CD4^{+} T cell response, which not only controls primary lesions but also limits metastasis by directly affecting the occurrence of metastasis-initiating disseminated cancer cells.[9–11] Subsequently, in a phase 1 clinical trial for HER2-positive (HER2^{pos}) breast cancer (BC), i.t. cDC1 immunotherapy with anti-HER2 antibodies, mediating antibody-dependent cellular cytotoxicity (ADCC) in the neoadjuvant setting, showed substantial tumor microenvironment (TME) reprogramming, robust responses, and clinical safety.[12] Despite these advancements, ongoing preclinical studies and clinical innovations for HER2^{pos} BC are mainly directed toward the utilization of anti-HER2 antibodies with chemotherapy, possibly associated with a high risk of adverse effects and variable treatment responses.[13–17] Therefore, to design safer next-generation immunotherapies against BC, which continues to be a major source of mortality among women and contributes to ~42,000 deaths with a 1% annual increase,[18] we explored the possibility of integrating antibody-based approaches to target unique tumor-related networks with existing cDC1 immunotherapy.

To this end, we focused on the interplay of tumor-intrinsic and -extrinsic factors that orchestrate an environment most

This is an open access article under the CC BY-NC license (http://creativecommons.org/licenses/by-nc/4.0/).

conducive for cancer cells to evade the host immune response.[19] The Semaphorin family exists as both transmembrane and soluble proteins and plays a dual role in the context of nervous system development and neuroinflammation, as well as influencing peripheral immune networks and cancer pathways.[20,21] Across various cancers, heightened expression of Semaphorin 4D (SEMA4D) acts as both a tumor-intrinsic and -extrinsic factor to remodel the TME and has been correlated with more aggressive disease.[22] SEMA4D expressed by tumor and immune cells can mediate myeloid-derived suppressor cell (MDSC) function and M2-polarized macrophage formation, which limit the anti-tumor immune response of immunotherapies and promote tumor growth.[23,24] Furthermore, SEMA4D expression at the tumor invasive margin has been reported to restrict the infiltration of antigen-presenting cells (APCs) and $CD8^+$ cytotoxic T lymphocytes (CTLs) into the tumor lesion. Disrupting this SEMA4D barrier increases intratumoral penetration of activated APCs and $CD8^+$ CTLs in tumors of syngeneic mouse models.[25] In clinical studies, SEMA4D neutralizing antibody also improved infiltration of CTLs and was noted to remodel myeloid suppression with favorable safety and tolerability.[26] Based on the widespread expression of SEMA4D in multiple solid tumors,[27] targeting SEMA4D could be instrumental in reshaping immune responses across multiple cancers, including BC.

Based on its robust expression in both leading-edge tumor cells and host immune cells, we hypothesized that in $HER2^{pos}$ BC, targeting SEMA4D may augment cDC1 immunotherapy. Impairment of SEMA4D activity in both compartments could provide dual relief, enhancing immune exchange between the TME and the immune system while also limiting myeloid suppressor cell-mediated immune suppression. Here, we investigated the effects of integrating anti-SEMA4D monoclonal antibodies (mAbs) with i.t. delivery of tumor-antigen-pulsed cDC1s in $HER2^{pos}$ BC syngeneic models. We performed a detailed analysis, ranging from *in vivo* efficacy to examination of the cellular interplay between these two therapies, to collect evidence in support of reshaping the primary and secondary tumor sites to produce a powerful anti-tumor response.

RESULTS

Blocking SEMA4D enhances DC immunotherapy

Based on the recently completed phase 1 trial of cDC1 immunotherapy for $HER2^{pos}$ BC patients,[12] we evaluated the combination of cDC1 immunotherapy and SEMA4D blockade in a subcutaneous $HER2^{pos}$ TUBO cell line BC model (Figure 1A). i.t. delivery of major histocompatibility complex (MHC) class II tumor-associated antigen-pulsed cDC1s (HER2 DC1s) with systemic delivery of anti-SEMA4D neutralizing mAb (αSema4D) resulted in complete tumor regression in 75% ($p \leq 0.0048$, Fisher's exact test, across two separate independent experiments) of TUBO-bearing mice along with a significant survival advantage compared to the group that received no therapy or monotherapies (Figures 1B–1D). An orthotopic mammary fat pad model also recapitulated the synergistic effect of SEMA4D blockade with tumor-directed cDC1s (Figures S1A and S1B). To determine its effectiveness against large tumors, we evaluated the combination therapy of HER2 DC1 with αSema4D in a high-tumor-burden subcutaneous TUBO model of $HER2^{pos}$ BC and found that the combination therapy more effectively attenuated tumor growth with survival benefits compared to monotherapies alone (Figures S1C and S1D). To test the efficacy of combination therapy against the *de novo* progression of HER2-positive mammary carcinoma, we utilized the BALB-HER2/neu model to demonstrate delayed progression of spontaneously arising tumors following HER2 DC1-αSema4D therapy (Figure S1E). To evaluate the clinical relevance of targeting human HER2 antigen, we assessed this combination therapy in the human HER2-expressing CT26 syngeneic model. Treatment with HER2 DC1 and αSema4D displayed significant efficacy of combination therapy compared to monotherapy or controls in this clinically relevant model (Figures S1F and S1G). As expected from previous findings, SEMA4D blockade showed a significant response in combination with checkpoint inhibitors. However, combining HER2 DC1 with αSema4D produced a significantly enhanced response compared to SEMA4D and checkpoint blockade (Figures S1H–S1J).

Previously, it has been reported that SEMA4D is strongly expressed at the invasive margins of tumors.[25] Immunofluorescence imaging from TUBO tumors confirmed the presence of a SEMA4D expression gradient, which co-localized with $KRT7^+$ epithelial tumor cells, suggesting tumor-specific expression of SEMA4D at the invasive margin, and was significantly attenuated with the combination of HER2 DC1 and SEMA4D blockade (Figure 1E). To examine the contribution of tumor-intrinsic SEMA4D in response to cDC1 immunotherapy, we generated SEMA4D-deficient TUBO cells (Figure S2). Intriguingly, the lack of SEMA4D specifically from the tumor compartment was associated with significantly slower tumor progression and enhanced response to HER2 DC1, providing supporting evidence for the pro-tumorigenic role of tumor-driven SEMA4D (Figures 1F and 1H). Notably, the attenuation of SEMA4D activity across a broader spectrum by systemic SEMA4D blockade in SEMA4D-deficient TUBO achieved significantly greater therapeutic potential for cDC1 immunotherapy, demonstrating synergistic effects of two SEMA4D compartments in tumor progression (Figures 1G–1I). Collectively, the data presented here support the increased efficacy of cDC1 immunotherapy following αSema4D treatment across various clinically relevant models, indicating that attenuation of both tumor and global SEMA4D is required to achieve an amplified response to cDC1 immunotherapy.

SEMA4D blocking triggers inflammatory reprogramming of the TME to facilitate cDC1 immunotherapy

To examine the reprogramming of the TME in response to SEMA4D blockade and i.t. delivery of HER2 DC1, we performed a bulk targeted transcriptome analysis of treated subcutaneous TUBO tumors, examining genes related to cancer pathways, immunology, metabolism, and myeloid innate immunity. HER2 DC1 treatment alone resulted in a significant upregulation of genes (107 genes), whereas αSema4D alone had little effect on upregulation (13 genes) when compared to the untreated control. However, combined with HER2 DC1, αSema4D resulted in a large change in upregulated gene expression (758 genes)

CellPress
OPEN ACCESS

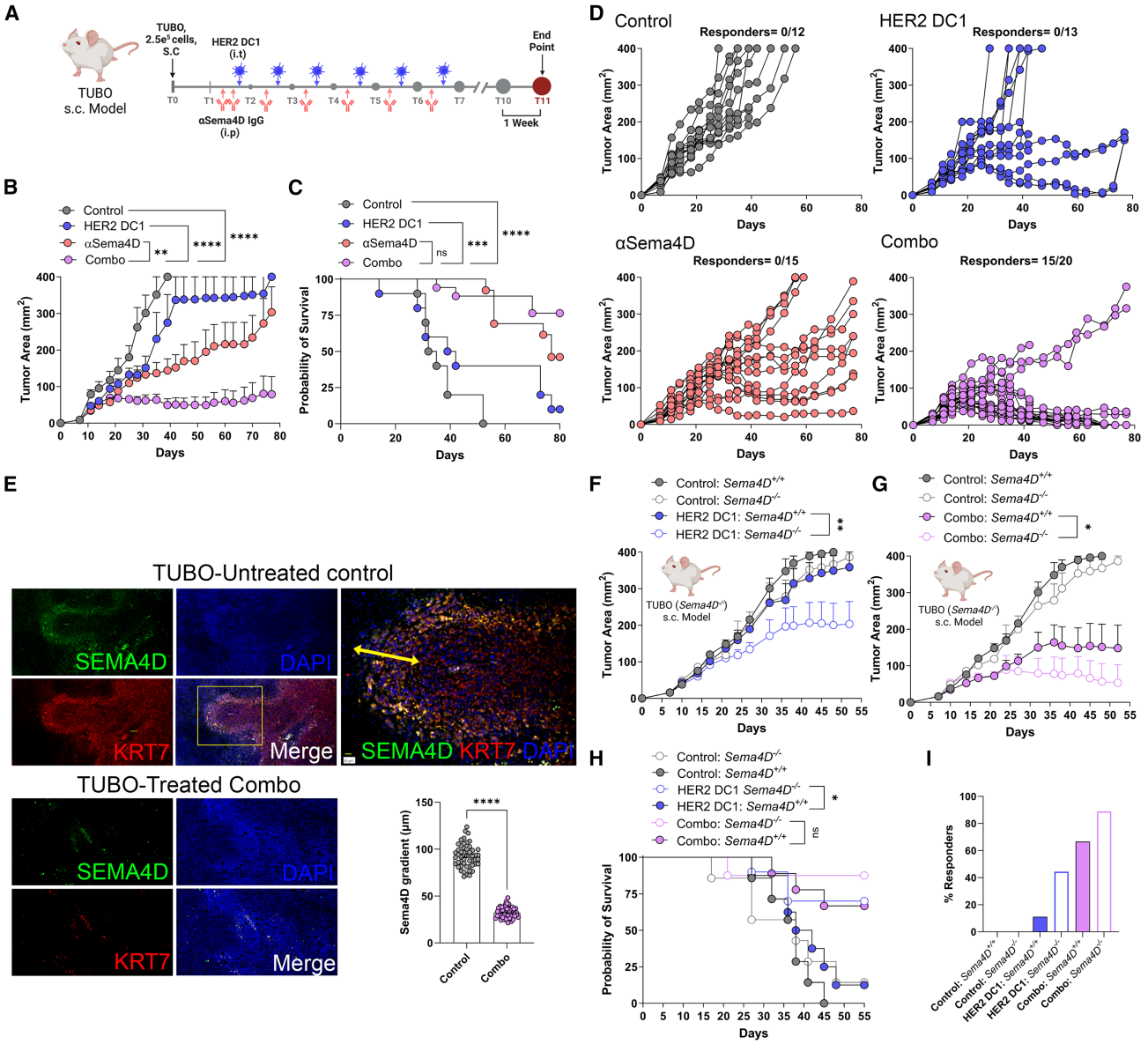

Figure 1. Intratumoral delivery of HER2 DC1 with αSema4D demonstrates robust efficacy in HER2^{pos} BC model

(A) Timeline of treatment of subcutaneous HER2^{pos} TUBO BALB/c model. Schematic showing the frequency of HER2 DC1 and αSema4D treatments.

(B) Mean tumor growth plots. Tumor growth was monitored with a caliper two times a week ($n = 10$ mice per group). Data are presented as mean ± SEM. Statistics using one-way ANOVA.

(C) Kaplan-Meier curve showing a significant effect of combination therapy on survival. Statistics using log-rank test.

(D) Individual tumor growth data of two separate experiments. Number of responder mice (with complete tumor regression) shown on top, based on the complete elimination of the visible tumor by caliper measurements at day 80.

(E) IF imaging from untreated TUBO tumors shows a gradient of SEMA4D expression on the invasive margins of the tumor. Treatment with i.t. HER2 DC1 and αSema4D significantly altered the SEMA4D gradient as shown by *x-y* measurements. Data are presented as mean ± SEM. Statistics using the Mann-Whitney test. Scale bar (high-magnification image), 20 μm.

(F–I) Efficacy of DC1 immunotherapy in SEMA4D CRISPR-KO of TUBO. (F and G) Mean tumor growth plots of WT mice implanted with WT and SEMA4D-deficient TUBO. Tumor growth was monitored with a caliper two times a week ($n = 9$ mice per group). (F) Comparing HER2 DC1 effect on tumor growth in WT and SEMA4D-deficient TUBO. Data are presented as mean ± SEM. Statistics using one-way ANOVA. (G) Combination treatment effect on tumor growth in WT and SEMA4D-deficient TUBO. Data are presented as mean ± SEM. Statistics using one-way ANOVA. (H) Kaplan-Meier curve of CRISPR-KO model. (I) Barplot showing the response rate of various treatments of CRISPR-KO model based on the response at day 40.

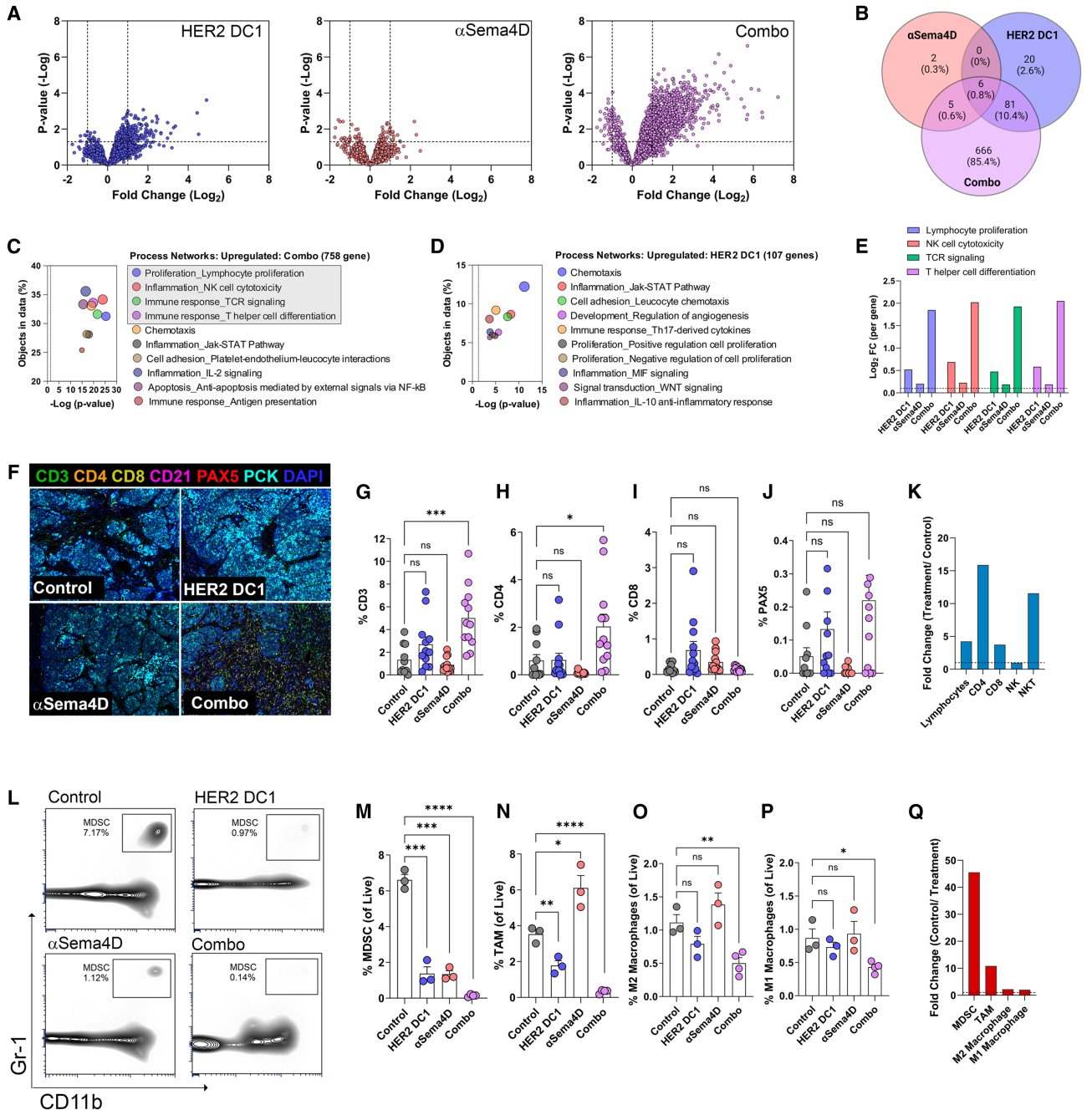

Figure 2. SEMA4D blockade reprograms TME to facilitate HER2 DC1-mediated anti-tumor immunity

(A) NanoString analysis from subcutaneous HER2^{pos} TUBO mice treated with HER2 DC1, αSema4D, and HER2 DC1+ αSema4D (combo) were compared to the no-treatment group (control) to examine the differential gene expression among different treatments based on 2-fold change with $p < 0.05$ (dotted lines).

(B) Venn diagram showing the number of genes in the upregulated dataset from different treatment groups in comparison to the no-treatment group (control).

(C–E) Enrichment analysis of the combination treatment was conducted using GeneGO in MetaCore. (C and D) Enrichment of the top ten process networks of upregulated datasets from the combination therapy and HER2 DC1 alone. The dotted line is $p = 0.05$. (E) Plot of $\log_2$ fold change per gene for process networks: lymphocyte proliferation (62 genes), NK cell cytotoxicity (67 genes), TCR signaling (60 genes), and T helper cell differentiation (71 genes) of HER2 DC1, αSema4D, and combo-treated tumors. The dotted line represents baseline expression.

(F) Multiplex-IF of mammary carcinoma collected from mice treated with different treatments. The malignant region is stained with αPan-cytokeratin (PCK).

(G–J) Quantification of immune populations from mIF. Twelve regions of interest were analyzed per condition using HALO. Data are presented as mean ± SEM. ns, not significant; *$p < 0.05$ and ***$p < 0.001$ by two-way ANOVA.

(K) Quantification of flow-cytometry data of fold increase of lymphocytes, CD4$^+$, CD8$^+$, NK, and NKT in HER2 DC1 + αSema4D mice in comparison to the control mice in TUBO model. The dotted line represents the baseline.

(legend continued on next page)

compared to the untreated control. Among upregulated genes, the majority (85%; 666 genes) were uniquely expressed by this combination (Figures 2A and 2B). Pathway analysis of the differentially expressed genes demonstrated enrichment in a broad spectrum of immunological networks, including lymphocyte proliferation, natural killer (NK) cell cytotoxicity, T cell receptor (TCR) signaling, T helper cell differentiation, and chemotaxis. On the contrary, HER2 DC1 alone showed only a limited effect on immunological networks, indicating that SEMA4D blockade strikingly unlocked the potential of cDC1 treatment (Figures 2C–2E), enhancing the expression of key processes involved in lymphocyte signaling and DC licensing, such as *Cd40*/*Cd40l* (Figure S3A). The combination treatment of HER2 DC1-αSema4D had a lower effect on down-regulating process networks related to cell-cycle and cancer-signaling pathways, such as NOTCH and WNT signaling, suggesting a limited effect on cancer progression directly (Figure S3B). We leveraged multiplex immunofluorescence (mIF) and flow cytometry to further evaluate the dynamic changes in the TME. The combination therapy increased the overall tumor-infiltrating lymphocyte (TIL) population (Figure 2F). Quantitative analysis of mIF images of 12 regions of interest from each treatment group revealed a significant increase in the overall $CD3^+$ T cell population (Figure 2G). A significant increase in $CD4^+$ T cells, but not in $CD8^+$ T cells, was observed in tumors treated with combination therapy, compared to tumors that received no treatment or monotherapies (Figures 2H and 2I). Flow-cytometry analysis of tumors was consistent with mIF (Figures 2K, S4A–S4E, and S5A). Notably, we did not observe significant changes in the B cell population via mIF ($PAX5^+$) or flow cytometry ($CD19^+$) (Figures 2F and S4F), consistent with the absence of mature tertiary lymphoid structure (TLS) via mIF. However, analysis of the 12-chemokine signature, which has been implicated in the formation of TLS in BC,[28] showed elevated levels of chemokine transcripts and corresponding higher TLS scores in response to combination therapy (Figure S4G).

The enrichment of the NK cell cytotoxicity process network in response to the combination therapy led us to examine the tumor-residing innate effector population. Surprisingly, we observed no significant changes in tumor-residing NK ($CD3^-CD49b^+$) cell populations in response to HER2 DC1-αSema4D therapy (Figures S4H and 2K). However, natural killer T (NKT)-like cells ($CD3^+CD49b^+$) showed a significant ∼10-fold increase in response to combination therapy compared with control tumors, which was mainly driven by cDC1 treatment (Figures S4I and 2K).

Next, we aimed to investigate whether the combination therapy led to enhanced memory responses and could establish a robust, self-sustaining anti-tumor immunity. Flow-cytometry analysis of treated tumors revealed that memory T cell populations showed a concomitant decrease in effector $CD4^+$ T cells and an increase in effector memory ($CD44^+CD62L^-$) $CD4^+$ T cells in response to HER2 DC1-αSema4D therapy, compared to the non-treated mice, with the majority of the effect being driven by HER2 DC1. In contrast, none of the treatments had an effect on the proportion of central memory ($CD44^+CD62L^+$) $CD4^+$ T cells (Figures S4J and S5). Among $CD8^+$ T cells, only central memory $CD8^+$ T cells showed a significant increase after combination therapy (Figure S4K). Consistent with these findings, rechallenged responder mice from the high-tumor-burden TUBO subcutaneous model showed protective immunity following tumor rechallenge (Figure S4L). These results strongly suggest that cDC1 immunotherapy can build strong critical memory responses.

To investigate the effect of treatments on pro-tumorigenic immune cell populations, we performed a multi-parametric flow-cytometry analysis of the myeloid cells in the subcutaneous TUBO model (Figure S5B). A significant ∼5-fold decrease in MDSCs was noted in mice receiving either HER2 DC1 or αSema4D monotherapies. Notably, in mice receiving the combination therapy, MDSCs were synergistically decreased ∼45-fold within the TME of responders (Figures 2L, 2M, and 2Q). Intriguingly, αSema4D alone increased the frequency of tumor-associated macrophages (TAMs); however, this trend was completely reversed following the integration of SEMA4D blockade with HER2 DC1 (Figures 2N and 2Q). Likewise, the number of M2 and M1 macrophages showed a slight reduction in frequencies in response to combination therapy compared to control and other treatment groups (Figures 2O–2Q). These findings demonstrate that cDC1 immunotherapy, in combination with SEMA4D blockade, has a robust impact on both anti- and pro-tumorigenic immune cells, shifting the balance toward a gain of effector and loss of inhibitory signals, thereby promoting immunological tumor regression.

SEMA4D blockade works through cDC1 cellular pathways of anti-tumor response contingent on early activation of the CD4 TH1 response

The changes in TME composition following HER2 DC1-αSema4D therapy prompted us to dissect the cellular mechanism of anti-tumor response. To examine the contributions of T cells and B cells to the therapeutic response, we utilized blocking antibodies to deplete $CD4^+$ T cells, $CD8^+$ T cells, and B cells individually in mice bearing subcutaneous TUBO tumors. The absence of $CD4^+$ T cells abrogated the tumor regression and survival benefit effects of combination therapy (Figure 3A). Depletion of $CD8^+$ T cells also limited the therapeutic effect of HER2 DC1 or αSema4D treatments, but only partially affected the therapeutic effect of combination therapy, suggesting a complementary role of $CD8^+$ T cells within the combination therapy (Figure 3B). Intriguingly, even though

(L) Flow plots showing the frequency of myeloid-derived suppressor cells (MDSCs) from control, HER2 DC1, αSema4D, and HER2 DC1 + αSema4D treatments. (M–Q) Immune profiling of myeloid phenotype by flow-cytometry analysis. Data are presented as mean ± SEM. ns, not significant; $^*p < 0.05$, $^{**}p < 0.01$, $^{***}p < 0.001$, and $^{****}p < 0.0001$ by *t* test. (M) Fraction of MDSCs of all viable cells ($CD11b^+GR\text{-}1^+$). (N) Fraction of tumor-associated macrophages (TAMs) of all viable cells ($CD11b^+F4/80^+$). (O) Fraction of M2 macrophages of all viable cells ($F4/80^+CD206^+$). (P) Fraction of M1 macrophages of all viable cells ($F4/80^+CD80^+$). (Q) Quantification of fold decrease of MDSCs, M1 macrophages, M2 macrophages, and TAMs in HER2 DC1 + αSema4D mice in comparison to the control mice in the TUBO model. The dotted line represents the baseline.

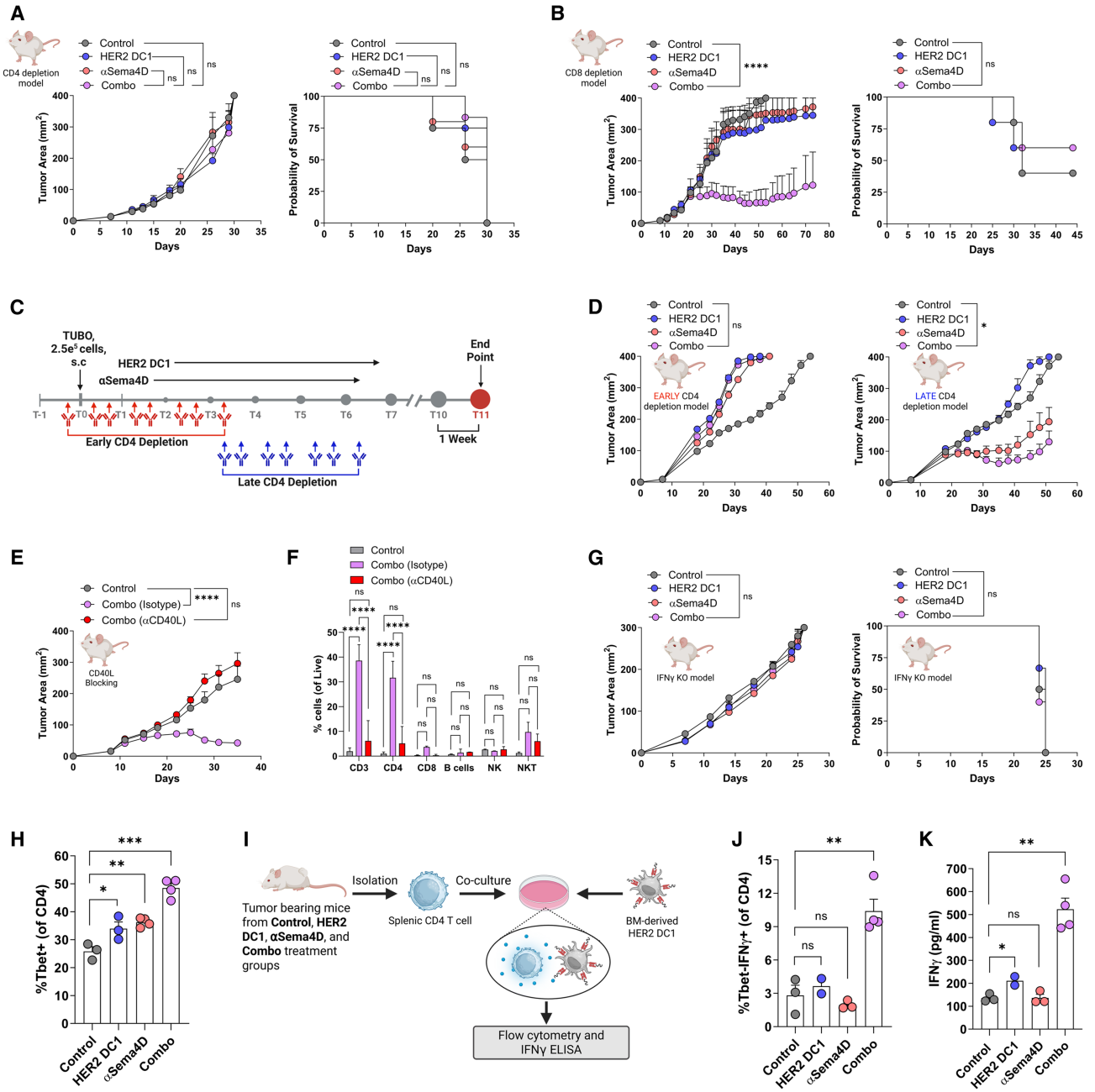

Figure 3. Sema4D blockade works through traditional cDC1 cellular pathways of anti-tumor response

(A) Tumor growth curves and survival curves of the CD4 T cell depletion model. After TUBO tumor establishment, mice received different therapies as indicated (n = 6 mice per group). Data are presented as mean ± SEM. Statistics using one-way ANOVA. Kaplan-Meier curve of the CD4 depletion model shows no significant effect of combination therapy on survival. Statistics using the log-rank test. Control mice were not treated with any treatments. The rest of the groups were subjected to CD4 depletion.

(B) Tumor growth curves and survival curves of the CD8 T cell depletion model. After TUBO tumor establishment, mice received different therapies as indicated (n = 8 mice per group). Data are presented as mean ± SEM. Statistics using one-way ANOVA. Kaplan-Meier curve of the CD8 depletion model showing no effect of the combination therapy on survival. Statistics using the log-rank test. Control mice were not treated with any treatments. The rest of the groups were subjected to CD8 depletion.

(C) Timeline displaying treatment doses of αCD4 antibody for early and late CD4 T cell depletion. For early depletion, BALB/c mice were injected with CD4 T cell depletion antibody 3 days prior to TUBO inoculation and continued two times a week until the completion of three monotherapy or three combination therapies in the TUBO tumor model. For late depletion, αCD4 antibody treatment was started from the fourth monotherapy or fourth combination therapy administration and continued until the completion of six monotherapies or six combination therapies in the TUBO tumor model.

(legend continued on next page)

there was no change in tumoral B cell frequency following HER2 DC1-αSema4D treatment, B cell depletion before tumor implantation resulted in a stunted response to combination therapy, suggesting that B cells functionally contributed toward the effect of the combination therapy (Figure S6A). We further dissected the significance of $CD4^+$ T cell activation timing on the therapeutic impact of combination therapy in the TUBO model. The early depletion of $CD4^+$ T cells completely eliminated the anti-tumor efficacy of the combination therapy. Interestingly, αSema4D and combination therapies provided partial protection, even in the absence of $CD4^+$ T cells, only until the fifth week of the model (Figures 3C and 3D). Since DC licensing of $CD4^+$ T cells required CD40, we next interrogated whether CD40 signaling is involved in the combination-therapy-mediated response. Impairing CD40-CD40L signaling via CD40L blocking antibody completely abolished the therapeutic efficacy of combination therapy and corresponded with a loss of $CD4^+$ T cells within the TME (Figures 3E and 3F). This dependency on $CD4^+$ T cells led us to conduct further investigation into the role of interferon-γ (IFN-γ) signaling, which is critical in mediating CD4 T helper 1 (Th1) differentiation.[29] Pathway analysis of expression data from tumors treated with HER2 DC1-Sema4D therapy revealed significant enrichment of IFN signaling and Th1 cell differentiation networks (Figure S6B). The absolute requirement of IFN-γ for the successful outcome of cDC1 immunotherapy provided the major evidence that type II IFN signaling is central to the therapeutic impact (Figure 3G). Furthermore, examination of the CD4 Th1 response within the tumor and in peripheral compartments revealed a significant boost in response to the combination therapy. Tumor-residing $CD4^+$ T cells showed a significantly higher frequency of T-bet expression (Figures 3H and S7A), and rechallenging the splenic $CD4^+$ T cells isolated from mice treated with HER2 DC1-αSema4D combination to HER2 peptide-pulsed DC1 resulted in a significant increase in the frequency of T-bet-expressing IFN-γ-positive cells, along with a significant boost in IFN-γ production (Figures 3I–3K and S7B), suggesting an amplified T helper state of TME and peripheral immune landscape. These findings demonstrate that the effects of combination therapy are primarily mediated by the early crosstalk between APCs and $CD4^+$ T cells, unlocking the IFN-γ-driven T helper response and engaging a more robust and effective anti-tumor response.

Priming of cDC1s within the TME is necessary for efficacious SEMA4D blockade

Immune infiltration data post i.t. HER2 DC1 and systemic αSema4D treatment strongly suggest that adoptively transferred mature cDC1s are central to the anti-tumor response, mediating the interplay of effector and inhibitory cues within the TME. Next, we aimed to investigate whether disrupting the SEMA4D expression gradient by systemic αSema4D treatment and subsequent increased trafficking of immune components within the TME would result in a similar level of sampling of tumor-specific antigens in a traditional vaccine paradigm, using subcutaneous delivery of cDC1s. We compared the combination therapy of HER2 DC1 delivered subcutaneously or intratumorally with systemic SEMA4D blockade and followed the tumor growth. Unlike i.t. HER2 DC1 therapy, subcutaneous HER2 DC1 combined with αSema4D failed to control tumors. Moreover, we observed a major loss of efficacy when immature DCs presenting MHC class II tumor antigens were used, suggesting that both i.t. delivery and the maturation status of adoptively transferred DCs were necessary to evoke the heightened anti-tumor response of HER2 DC1 and SEMA4D blockade (Figures 4A and 4B). To examine immune cell infiltration following subcutaneous HER2 DC1 delivery in combination with SEMA4D blockade, we performed flow cytometry of treated tumors (Figure 4C). Unlike i.t. delivery, the subcutaneous route showed no significant changes in tumor-infiltrating T cells. Notably, only the NKT population showed a significant increase within the combination group compared to the control, although the difference was minor compared to that observed with i.t. delivery of cDC1s. subcutaneous delivery of cDC1s did not elicit any changes in other immune populations, such as the NK and B cell populations (Figure 4D). In addition, subcutaneous HER2 DC1 with SEMA4D blockade failed to elicit an optimal immune response, thereby limiting the myeloid-cell population, including MDSCs and TAMs (Figure 4E). Overall, these findings demonstrate that i.t. delivery of DCs is critical to elicit a balanced anti-cancer immune response following combination therapy.

Blocking SEMA4D supports the systemic anti-tumor response with active migration of primed cDC1s to secondary lesions

A heightened CD4 Th1 response in the peripheral compartment, originating from the TME, prompted us to investigate

(D) Tumor growth of the EARLY and LATE CD4 depletion model ($n = 7$ mice per group). Data are presented as mean ± SEM. Statistics using one-way ANOVA. Control mice were not treated with any treatments. The rest of the groups were subjected to CD4 depletion.

(E) Intact CD40-CD40L signaling is essential for the therapeutic effect of HER2 DC1-αSema4D therapy ($n = 8$ mice per group). Data are presented as mean ± SEM. Statistics using one-way ANOVA.

(F) Effect of impairment of CD40-CD40L signaling on recruitment of lymphocytes, $CD4^+$ T cells, $CD8^+$ T cells, B cells, NK cells, and NKT cells in HER2 DC1 and αSema4D combination therapy mice. Data are presented as mean ± SEM. ns, not significant; $^{****}p < 0.0001$ by *t* test.

(G) Tumor growth curves and survival curves of IFN-γ KO mice bearing subcutaneous TUBO tumors. After tumor establishment, mice were treated with HER2 DC1 alone or αSema4D antibody alone or in combination ($n = 8$ mice per group). Control and HER2 DC1 data were reproduced from Jia et al.[30] Data are presented as mean ± SEM. Statistics using one-way ANOVA. Kaplan-Meier curve of the IFN-γ KO model shows no significant effect of combination therapy on survival, using the log rank test.

(H–K) Measurement of tumor and peripheral Th1 response following cDC1 immunotherapy. (H) Frequency of T-bet-expressing CD4 T cells within the tumor estimated by flow cytometry. Data are presented as mean ± SEM. $^*p < 0.05$, $^{**}p < 0.01$, $^{***}p < 0.001$ by *t* test. (I) Schematic showing the experimental design to perform *in vitro* co-culture of DC1 with splenic $CD4^+$ T cell to record anti-HER2 response. (J) Frequency of T-bet-IFN-γ double-positive $CD4^+$ T cells from co-culture experiment. Data are presented as mean ± SEM. ns, not significant, $^{**}p < 0.01$ by *t* test. (K) Measurement of IFN-γ by ELISA. Data are presented as mean ± SEM. ns, not significant. $^*p < 0.05$, $^{**}p < 0.01$ by *t* test.

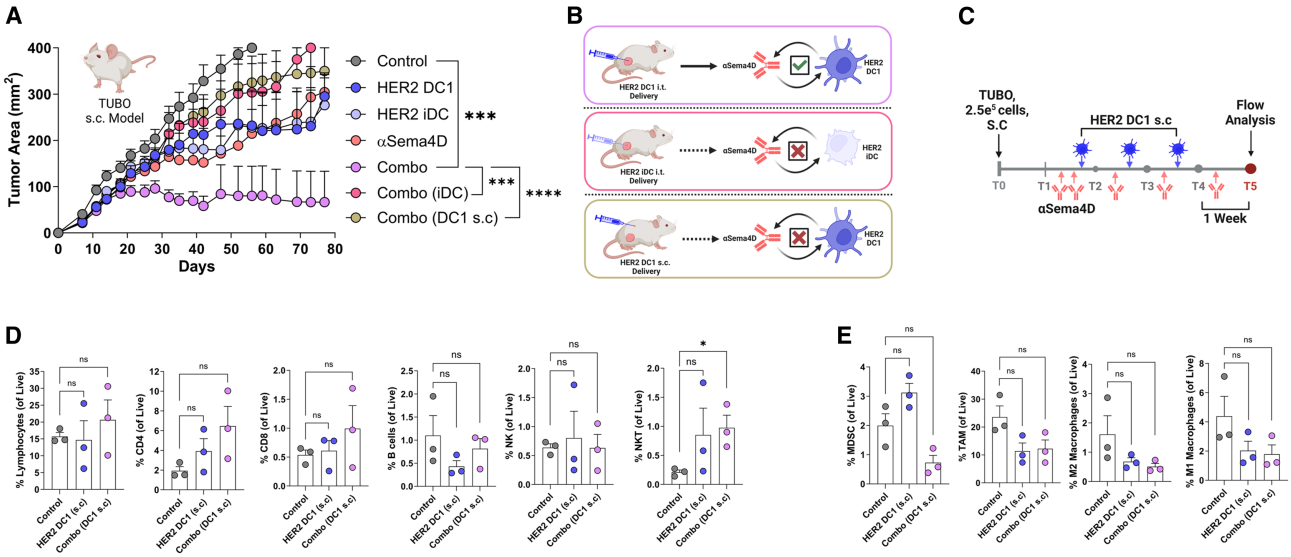

Figure 4. Priming of cDC1s within the TME is necessary for efficacious SEMA4D blockade

(A) Testing of different delivery methods and maturity status of cDC1s in the subcutaneous TUBO model to examine the prerequisite conditions of response to combination therapy. Mice were treated as indicated (n = 8 mice per group). Data are presented as mean ± SEM. Statistics using one-way ANOVA.

(B) Schematic showing the prerequisite conditions for optimal crosstalk between HER2 DC1 and SEMA4D blockade.

(C) Timeline of treatments of subcutaneous TUBO BALB/c model to show flow-cytometry analysis time point.

(D) Immune profiling of effector phenotype of tumor-infiltrating lymphocytes by flow-cytometry analysis. Data are presented as mean ± SEM. ns, not significant; $^{*}p < 0.05$ by t test. Fraction of lymphocytes, CD4, CD8, NKT, NK, and B cells of all viable cells.

(E) Immune profiling of myeloid cells within TME by flow-cytometry analysis. Data are presented as mean ± SEM. ns, not significant; p value by t test. Fraction of MDSCs, TAMs, M1 macrophages, and M2 macrophages of all viable cells.

whether cDC1 immunotherapy elicits systemic immunity. To address this, we utilized a HER2^{pos} TUBO subcutaneous BC bilateral model and treated only the left flank tumor with HER2 DC1. Remarkably, within the combination treatment group, untreated tumors identical to treated tumors in 75% of mice demonstrated complete regression ($p \leq 0.007$, Fisher's exact test), and these mice had a significant survival advantage compared to mice that received no therapy or only monotherapies (Figures 5A and 5B), suggesting that HER2 DC1-αSema4D combination therapy provided an abscopal anti-tumor effect.

Similar tumor regression kinetics of treated versus untreated tumors prompted us to speculate on the overlapping interplay of immune players at both lesions. To examine the overlap between untreated and treated TME, we performed targeted transcriptome analysis on untreated tumors. Robust correlations of gene-expression data for composite analysis and individual NanoString panels were noted, suggesting an overlapping mechanism of therapeutic effect leading to tumor regression on both flanks (Figures 5C and S8). Consistently, pathway enrichment analysis also demonstrated similar and significant enrichment of process networks in both tumors (Figure 5D). To further evaluate the overlap of the cellular mechanism of the abscopal effect, we performed flow-cytometry analysis to characterize the immune populations in the untreated flank. Consistent with transcriptome data, TILs and the myeloid suppressor cell population in the untreated tumor show a similar profile that was noticed for treated lesions (Figures 5E, 5F, and S9A–S9J). Robust molecular and cellular overlap between treated and untreated tumors strongly suggested a similar priming mechanism mediated by tumor-antigen-presenting cDC1s at both lesions. Moreover, pathway enrichment analysis identified chemotaxis as one of the most enriched process networks following both HER2 DC1 alone and HER2 DC1-αSema4D treatment on both primary and secondary tumor lesions (Figures 5D and S10A). Therefore, we sought to investigate whether there is active trafficking of i.t. cDC1s to secondary tumor lesions and lymph nodes. We injected CellTrace Violet (CTV)-labeled HER2 DC1s into the left flank tumor in the bilateral tumor model and measured the fraction of labeled cells that migrated to the untreated flanks at 24 and 48 h (Figures 5G and S11). As anticipated, after 24 h, CTV-labeled cDC1s were detected in the treated flank in both HER2-DC1-alone and combination-therapy mice. In the untreated flank, we observed an increased migration of labeled cDC1s after 24 h in the combination therapy compared to the HER2 DC1s alone, suggesting that αSema4D enhances cDC1 trafficking to distal tumor sites (Figure S10B). Increased cDC1 trafficking in the untreated flank was observed and sustained up to 48 h after cDC1 administration (Figure 5H). Similarly, an increase in labeled cDC1 trafficking to the draining lymph nodes on both treated and untreated flanks was noted in the combination therapy compared to the HER2 DC1 monotherapy mice 24 and 48 h after labeled cDC1 delivery (Figures S10C and 5I). Notably, migration of labeled cDC1s to non-draining lymph nodes was also enhanced with combination therapy 48 h post cDC1 delivery, suggesting the necessity of SEMA4D blockade to display the full spectrum of abscopal effect (Figures S10D and 5J).

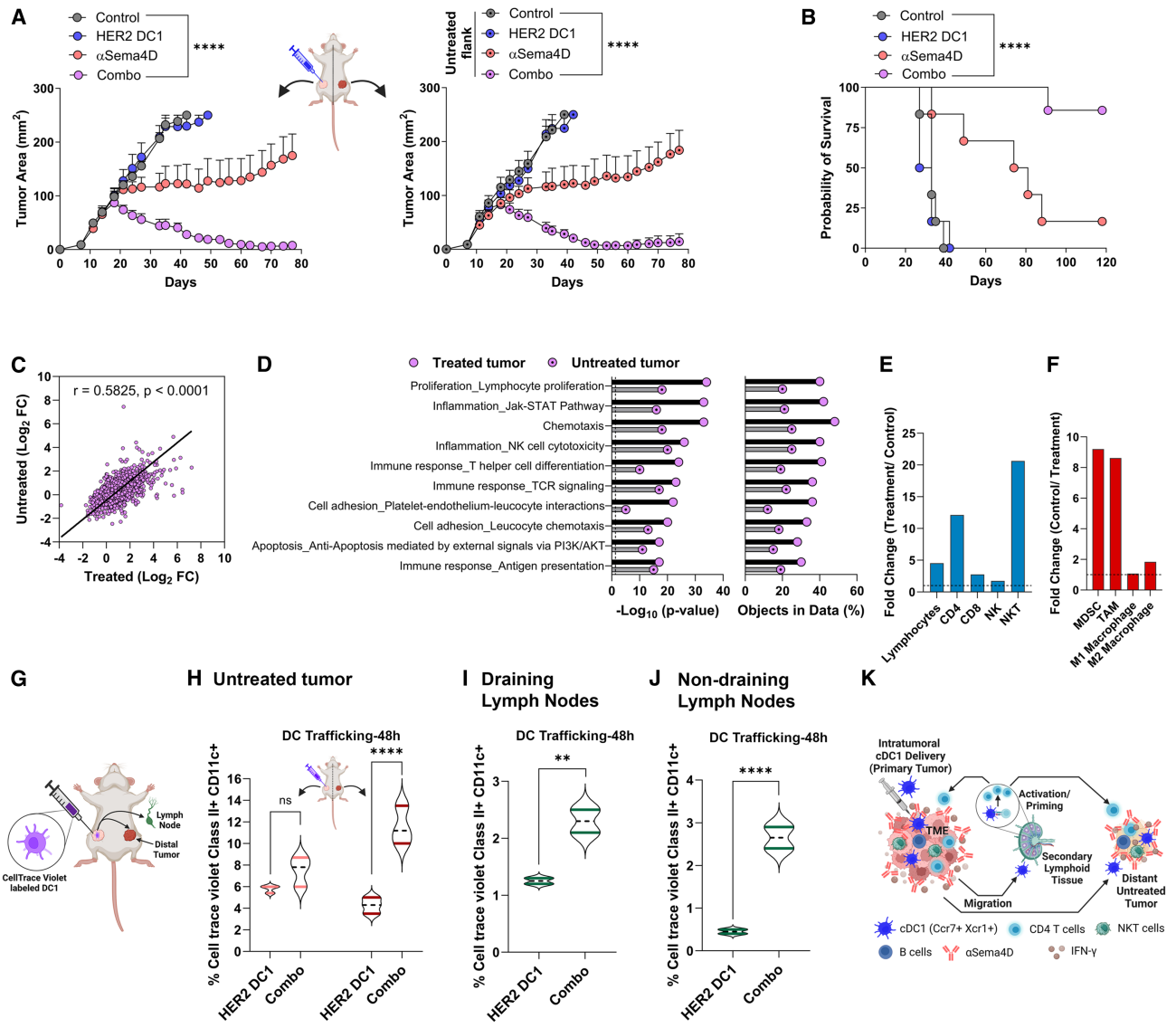

Figure 5. Blocking Sema4D supports the systemic anti-tumor response of HER2 DC1 therapy with active migration of primed cDC1s to secondary lesions

For the bilateral tumor model, BALB/c mice were inoculated with TUBO cells subcutaneously on both flanks. Intratumoral HER2 DC1 doses were administered only on the left flank tumors.

(A) Tumor growth ($n = 8$ mice per group). Tumor growth curves of treated flank (left) and untreated flank (right). Data are presented as mean ± SEM. Statistics using one-way ANOVA. In these tumor growth curves, only responder mice were plotted to show the tumor regression kinetics of both treated and untreated flanks.

(B) Kaplan-Meier curve shows a significant effect of combination therapy on the survival of the bilateral tumor model. Statistics using the log-rank test.

(C) Scatterplot of combined gene-expression changes of four NanoString panels of treated and untreated tumor flanks of HER2 DC1-αSema4D treated mice. Statistics using Pearson correlation.

(D) Comparison of enrichment analysis of treated and untreated tumor flanks using GeneGO showing enrichment of the top ten process networks of upregulated datasets. The dotted line is $p = 0.05$.

(E) Quantification of fold increase of lymphocytes, $CD4^+$ T cells, $CD8^+$ T cells, NK cells, and NKT cells in the untreated flank of HER2 DC1-αSema4D treated mice in comparison to the control mice. The dotted line represents the baseline.

(F) Quantification of fold decrease of MDSCs, TAMs, M1 macrophages, and M2 macrophages in the untreated flank of HER2 DC1-αSema4D treated mice in comparison to control mice. The dotted line represents the baseline.

(G) Schematic showing experimental layout to trace the trafficking of labeled DC1 to the distal tumor site and lymph nodes.

(H) Labeled cDC1 trafficking to the distal (untreated) tumor in the bilateral TUBO model. CellTrace violet-labeled cDC1s was administered to the left flank (treated) tumor of HER2 DC1-treated and HER2 DC1-αSema4D-treated mice ($n = 2$). Following the labeled DC1 dose, both treated and untreated tumors were analyzed to examine the presence of labeled cDC1s after 48 h. Data are presented as mean ± SEM. ns, not significant; $^{****}p < 0.0001$ by two-way ANOVA.

(I) Labeled cDC1 trafficking to draining lymph node (DLN). CellTrace Violet-labeled cDC1s were examined in DLN of HER2 DC1-treated and HER2 DC1-αSema4D treated mice ($n = 2$) after 48 h of cDC1 administration in the primary tumor site. Data are presented as mean ± SEM. $^{**}p < 0.01$ by two-way ANOVA.

(legend continued on next page)

These findings strongly indicate an active migration loop of antigen-presenting machinery from the primary tumor site to secondary sites, including lymph nodes and even distal tumors. Based on current findings, we claim that SEMA4D blockade is pivotal in supplementing DC function to prime and operate this loop to elicit a similar anti-tumor abscopal effect (Figure 5K).

Clinical relevance of targeting SEMA4D for BC

Analysis of publicly available gene-expression data from The Cancer Genome Atlas (TCGA) indicated that SEMA4D is a putative target in human BC, with significantly higher mRNA expression in tumors compared to normal tissue (Figure 6A). To confirm this enhanced SEMA4D protein expression and compare different subtypes of BC, we performed mIF on clinical specimens from HER2^{pos} BC and triple-negative BC (TNBC) patients. The HER2^{pos} BC cohort showed robust SEMA4D protein expression in both stromal and tumor compartments, which was significantly higher than the SEMA4D expression in TNBC specimens (Figure 6B). Interestingly, 4T1, a syngeneic model of TNBC, recapitulated the clinical specimens, expressing SEMA4D at much lower levels compared to TUBO (Figures S12A and S12B). Consistent with lower SEMA4D expression, combining cDC1s presenting tumor-associated class II antigens (HER3 DC1s, based on overexpression of HER3 in TNBC) with SEMA4D blockade in the 4T1 model only provided marginal benefit over the cDC1 monotherapy group (Figure S12C). Thus, tumor intrinsic expression of SEMA4D may be a robust predictor of the response to αSema4D.

Next, we assessed the potential clinical feasibility of utilizing SEMA4D blockade for HER2^{pos} BC by replacing one αHER2 antibody in the dual trastuzumab/pertuzumab combination to provide a safer cDC1 immunotherapy option. Expectedly, the HER2 DC1-trastuzumab combination showed significant and rapid tumor regression in syngeneic orthotropic HER2^{pos} tumors, which was similar to the effect of HER2 DC1-αSema4D. However, the strongest responses were observed when we combined systemic αSema4D with HER2 DC1-trastuzumab (Figure 6C). Combining SEMA4D blockade with HER2 DC1-trastuzumab also translated to a significant increase in overall survival (Figure 6D). Furthermore, the HER2 DC1-trastuzumab+ αSema4D combination showed the highest response rate of ~85% among all treatments, which was even more effective than the response rate of ~75% of HER2 DC1s in combination with both trastuzumab and pertuzumab in the HER2^{pos} TUBO model[10] (Figures 6E and 6F).

Collectively, the findings presented here uncovered the robust role of SEMA4D blockade in reprogramming the TME to augment cDC1 immunotherapies. Based on these findings, prospective clinical trials for BC patients could have great clinical implications, providing evidence that SEMA4D blockade can successfully be integrated with existing immunotherapies in clinical settings to deliver a safer and more effective therapy.

DISCUSSION

Repurposing activated cDC1s from their traditional role as vaccines to agents of direct reprogramming of the TME to create an environment favorable for tumor eradication has reinvigorated BC DC immunotherapies.[12] However, to enhance the potency of neoadjuvant frontline i.t. cDC1 therapy, first, we needed an agent capable of enhancing active influx of immune effectors into the TME, which is not only crucial for successful immunotherapy but also linked to more favorable outcomes of subsequent chemotherapy in many cancers, including BC.[31–33] Second, disrupting the protumorigenic responses driven by cells of myeloid origin, such as MDSCs and TAMs, which represent a substantial resistance mechanism by promoting cancer cell proliferation, angiogenesis, and host immunosuppression,[34–37] can supplement the outcomes of a variety of immunotherapies. Dichotomy of SEMA4D expression in tumor and its effects on myeloid suppressor cells provided an ideal candidate to target these two requirements: to breach a physical barrier generated by tumor-expressing SEMA4D and to impair the expansion and suppressive function mediated by SEMA4D.[23–25,38,39] Indeed, the integrated approach of adoptive transfer of activated cDC1s with SEMA4D blockade was highly effective across a number of models and outperformed checkpoint blockade. The significant dependency of anti-tumor response on tumor-expressing SEMA4D confirmed the synergistic interplay of both tumor-intrinsic and -extrinsic SEMA4D in escaping immune surveillance in response to immunotherapies. Likewise, the combination of cDC1s and SEMA4D blockade not only dismantled the SEMA4D-driven physical barrier but also synergistically eliminated MDSCs and M2 macrophages from the tumor, which we posit is the driving force behind the sustained anti-tumor response that effectively eliminates HER2-positive BC tumors.[40–42]

The reprogrammed TME facilitated the early sensitization of the CD4$^+$ T cell response mediated by adoptively transferred activated cDC1s and the contribution of B cells to generate potent anti-tumor immunity.[43,44] In addition, intact CD40-CD40L signaling is essential for a favorable outcome of the combination therapy, which is critical for the CD4$^+$ T-cell-mediated helper response to license DCs to induce productive CD8 cytotoxic responses.[45–47] Notably, SEMA4D is expressed on a variety of immune cells, including T cells, which is reported to signal to receptors on DCs to enhance DC maturation and T cell priming.[48,49] We believe SEMA4D blockade does not adversely affect immune priming in these studies because we bypassed the early DC priming by adoptively transferring preactivated cDC1s within the TME, providing a rationale for why the two approaches are particularly well matched. This is further supported by the fact that variation in either maturation status or delivery route of adoptively transferred DCs severely affects the synergy between these approaches. Matured DCs present within a TLS of a tumor create an optimal Th1 immune landscape to stimulate positive immune response,[50] which is associated with a favorable response to immunotherapy across various

(J) Labeled cDC1 trafficking to non-draining lymph node (nDLN). CellTrace Violet-labeled cDC1s were examined in nDLN of HER2 DC1 and HER2 DC1-αSema4D mice (n = 2) after 48 h of cDC1 administration in the primary tumor site. Data are presented as mean ± SEM. ****$p < 0.0001$ by two-way ANOVA.
(K) Schematic showing the cellular mechanism of HER2 DC1-αSema4D therapy to tip the balance in favor of immune recognition of primary and distant tumors to attain systemic anti-tumor immunity.

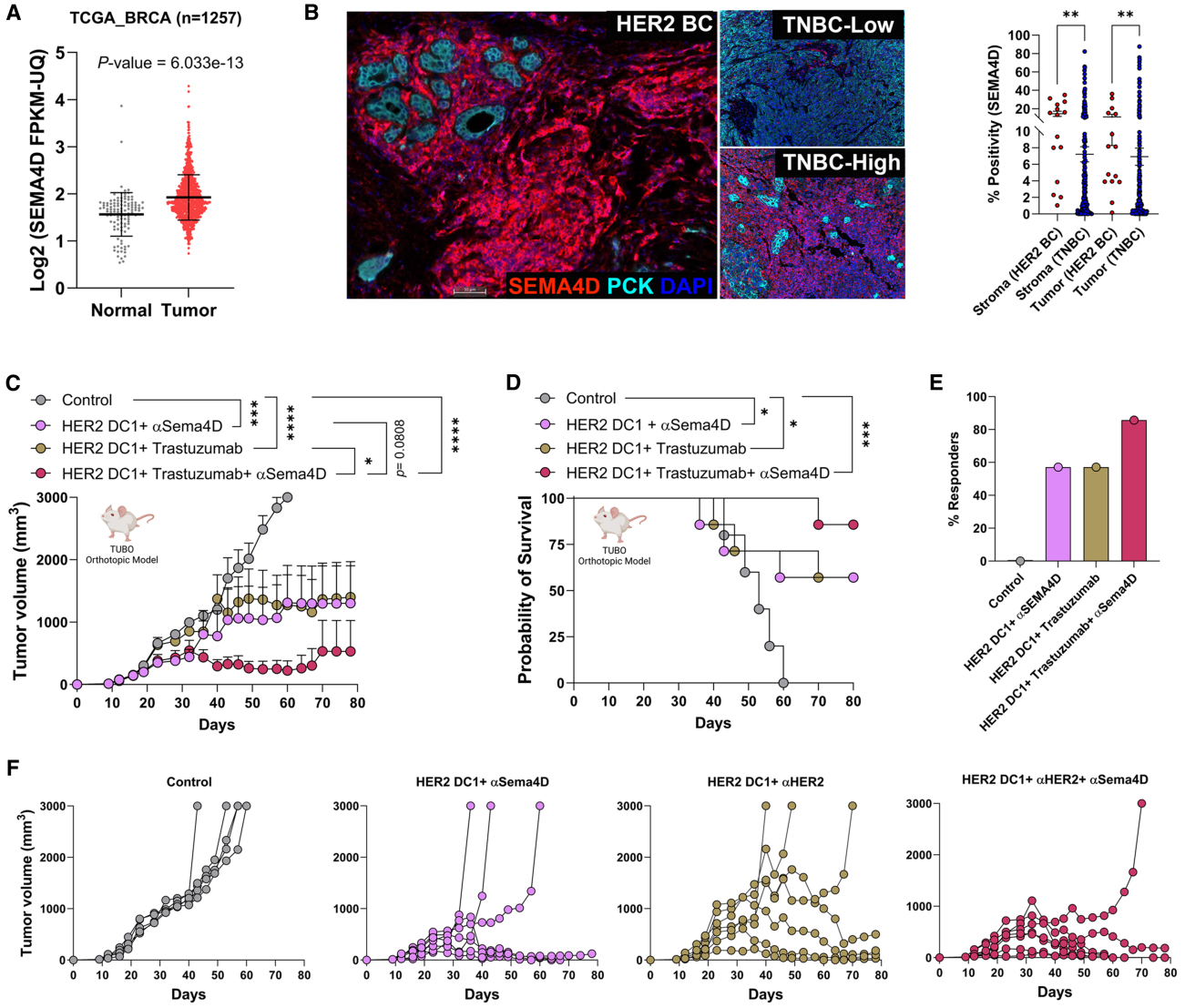

Figure 6. Clinical relevance of targeting SEMA4D for BC

(A) Genomic analysis of the TCGA database of breast cancer patients showing SEMA4D mRNA expression in BC patients from normal and malignant tissues. Data are presented as mean ± SD. Statistics by *t* test.

(B) Representative mIF micrographs showing SEMA4D expression from specimens from HER2^{pos} and TNBC patients. HALO analysis of mIF images from HER2^{pos} (n = 15) and TNBC (n = 90) patients to show positivity of SEMA4D in two subtypes of BC. Both stromal and tumor compartments were analyzed for SEMA4D expression. Data are presented as mean ± SEM. $^{**}p < 0.01$ by Kruskal-Wallis test.

(C–E) Effect of integrating SEMA4D blockade with HER2 DC1+ αHER2 (trastuzumab) therapy. (C) Tumor growth (n = 7 mice per group). Data are presented as mean ± SEM. Statistics using one-way ANOVA. (D) Kaplan-Meier curve showing a significant effect of combination therapy on survival. Statistics using the log-rank test. (E) Barplot depicting the response rate of various treatments.

(F) Individual tumor growth plots from the different treatment groups.

cancers.[50–54] Although we did not observe a TLS in response to adoptively transferred, preactivated cDC1s with SEMA4D blockade, possibly due to the inherent limitations of detecting mature TLS formation in murine models,[55] the enrichment of a 12-chemokine TLS signature following combination therapy suggested a possible interplay of immune cells to initiate the TLS formation.

A systemic response is necessary to achieve the full therapeutic potential of immunotherapies.[56] Remarkably, SEMA4D blockade reprogrammed the untreated distal tumors to receive immune signals from primary lesions, producing a strikingly similar immune landscape driven by migrated, activated cDC1s within the lymph nodes and at the secondary tumor sites. Mechanistically, the IFN-γ-dependent CD4 TH1 response appears to be driving this systemic effect, evident from increased frequency of peripheral T-bet-expressing IFN-γ-producing CD4^{+} T cells following combination therapy. IFN-γ secreted by CD4^{+} T cells can participate in tumor elimination through

cytotoxicity, inhibiting angiogenesis, promoting senescence (especially in disseminated cancer cells), and inhibiting migration in a variety of cancer cells.[11,30,57–61] Notably, depletion of $CD4^+$ T cells in the late phase of the model provided only partial protection until the fifth week, after which a relapse was noticed in several mice, indicating involvement of the tumor-resident $CD4^+$ T cell effector memory response in the late phase of tumor clearance, which plays a pivotal role in providing sustained tumor immunity.[62,63] Despite the loss of effectiveness of DC1 immunotherapy due to a lack of $CD4^+$ T cells in the late phase, a partial response suggested an interplay of other effectors in controlling tumor progression. Interestingly, partial loss of effectiveness of the integrated approach in the $CD8^+$ T cell depletion model also coincides with late $CD4^+$ T cell depletion, suggesting a supplementary role for $CD8^+$ T cells in anti-tumor immunity during the late phase. Apart from the conventional T cell repertoire, a population of innate effector NKT cells bearing anti-tumor properties was significantly enriched following combination therapy.[64,65] NKT cells participate in anti-tumor responses by recognizing glycolipid targets in the context of the non-classical MHC molecule, CD1d, and responding by secreting cytokines, including IFN-γ and tumor necrosis factor α.[66–69] Thus, it was not surprising to see that the efficacy of the integrated approach was absolutely dependent on the availability of IFN-γ to provide both early and sustained systemic anti-tumor immunity mediated by a variety of immune effector cells. Currently, we are investigating the synergy between several processes to enhance innate anti-tumor-signaling pathways in response to cDC1 immunotherapy.

In addition to the immunomodulatory effects of SEMA4D blockade, SEMA4D blockade may also have direct impacts on cancer signaling pathways, thereby limiting tumor progression and metastasis. A number of studies have implicated elevated SEMA4D with tumor aggressiveness and poor prognosis to the standard-of-care treatment in cancer patients.[22,70–74] SEMA4D mediates signaling through its high-affinity cognate receptor, Plexin B1 (PLXNB1), expressed on APCs and non-lymphoid tissue, including tumor cells.[75,76] SEMA4D-PLXNB1 crosslinking can activate cMET and ERBB2 oncogenic signaling to promote tumor progression.[72,73,75,77] Interestingly, targeted transcriptomics analysis revealed a limited effect on tumor-promoting networks, suggesting that the combination of cDC1s and SEMA4D blockade exerts a predominantly immunomodulatory effect rather than an anti-oncogenic effect.

TCGA and mIF data demonstrated that SEMA4D is overexpressed in malignant BC tissue. Moreover, heightened expression in a majority of $HER2^{pos}$ BC and some TNBC patients supported a case for targeting SEMA4D with pepinemab, a humanized version of SEMA4D neutralizing mAb, which is already under clinical investigation for a number of indications, including cancer and neurodegenerative diseases.[26,78] Based on current findings demonstrating enhanced efficacy and the favorable safety profile of pepinemab, we believe that SEMA4D is a putative target in HER2 BC and anticipate incorporating well-tolerated pepinemab with existing targeted therapies and perhaps replacing more toxic HER2-targeting antibodies, specifically pertuzumab.[13,14,26] The addition of SEMA4D blockade to i.t. cDC1s in combination with trastuzumab showed promising effects by strongly increasing the frequencies of therapy responders in $HER2^{pos}$ models. Judicious targeting of SEMA4D in low/heterogeneously HER2-expressing BC also provides an improved avenue for cDC1 immunotherapy. Furthermore, the overexpression of SEMA4D across multiple tumor types, along with a high frequency of MDSCs, warrants further testing to examine the feasibility of incorporating pepinemab with cDC1 immunotherapy for various cancers.[27] Largely, the findings presented here have promising translational implications for leveraging DCs to design next-generation cancer immunotherapies.

Limitations of the study

We acknowledge several limitations that warrant careful consideration and further investigation. First, the mechanistic insights are mainly derived from murine models, which may not fully recapitulate the complexity of the human tumor, particularly with respect to B cell function, tertiary lymphoid structure formation, and myeloid-cell subsets.[79–81] Therefore, future studies targeting these interactions in patient specimens would be necessary to further elucidate the mechanistic interplay between activated cDC1s and SEMA4D blockade. Second, despite the robust synergy of the integrated approach, TME remodeling depends on tumor-expressed SEMA4D, potentially limiting its applicability in tumors with low or heterogeneous SEMA4D expression. The successful immune response relied on multiple effector populations, including $CD4^+$ T cells, $CD8^+$ T cells, and NKT cells, making the therapeutic effect vulnerable to variability in host immune composition or function. Finally, although the efficacy of intratumoral cDC1 immunotherapy with SEMA4D blockade is largely established in the preclinical $HER2^{pos}$ (TUBO) model, this would need to be tested in patients. However, we have observed a high reproducibility of preclinical findings in HER2-positive BC patients with previous DC-based preclinical approaches; therefore, we anticipate a favorable outcome of pepinemab dosing and integration with intratumoral cDC1 immunotherapy in future clinical trials.

RESOURCE AVAILABILITY

Lead contact

Requests for additional information, resources, or reagents should be directed to the lead contact, Dr. Brian J. Czerniecki (brian.czerniecki@moffitt.org).

Materials availability

All unique reagents used in this study are available upon request following completion of a materials transfer agreement with the Moffitt Cancer Center.

Data and code availability

- The RNA transcript data produced in this study are publicly available through the Gene Expression Omnibus (GEO). Accession numbers for individual NanoString panels are PanCancer, GEO: GSE302765; Immunology, GEO: GSE302764; Myeloid Innate Immunity, GEO: GSE302763; and Metabolic Pathways, GEO: GSE302735. GEO accession numbers are also listed in the key resources table.
- No original code is reported with this study.
- Any additional information related to the data reported in this paper is available from the lead contact upon request.

ACKNOWLEDGMENTS

This work was supported by the Department of Defense award W81XWH-16-1-0385 to B.J.C. This work was also supported by Shula Breast Cancer Research

Fund, awarded to B.J.C. and Pennies in Action, awarded to B.J.C. This work was supported in part by the Small Animal Imaging Lab, Flow Cytometry Core, Molecular Genomics Core, Biostatistics and Bioinformatics Shared Resource, Tissue Core Histology, Analytic Microscopy Core, and Vivarium Services at the Moffitt Cancer Center, an NCI-designated Comprehensive Cancer Center (P30-CA076292). We thank Dr. Shari Pilon-Thomas (H. Lee Moffitt Cancer Center & Research Institute) for providing BALB/c-HER2/neuT transgenic mice. Technical assistance from Jaqueline Cortez, Grace Spiegelhoff, Sy Olson-Mcpeek, Isabella Valenzuela, and Vishnu Indukuri is duly acknowledged.

AUTHOR CONTRIBUTIONS

Conceptualization, S.K.G., K.N.K., C.S., G.R., E.E.E., G.K.K., and B.J.C.; methodology & investigation, C.S., S.K.G., G.R., K.N.K., V.L., A.L.A., E.E.E., H.B., J.V.N., J.Y., A.B., N.G., D.W., J.A.V.M., and D.C.C.; visualization, S.K.G., C.S., K.N.K., and G.R.; funding acquisition, B.J.C.; project administration, S.K.G., K.N.K., P.C.R., and B.J.C.; supervision, S.K.G., K.N.K., and B.J.C.; writing – original draft, S.K.G., K.N.K., C.S., G.K.K., and B.J.C.; writing – review & editing, G.R., A.L.A., D.W., V.L., M.Z., and E.E.E.

DECLARATION OF INTERESTS

Application US18/307,920 was held by Moffitt and Vaccinex Inventors "Combination therapy with semaphorin-4D blockade (SEMA4D) and DC1 therapy." The application was granted in January 2025: B.J.C., K.N.K., and E.E.E. A patent application is filed with ImmunoRestoration for intellectual property on a human version of cDC1s: G.K.K. and B.J.C. Vaccinex employment and stock: E.E.E., H.B., and M.Z. Vaccinex patents and applications are related to SEMA4D (USPTO nos. 8,816,058, 9,090,709, 10,800,853, and 7,919,594).

STAR★METHODS

Detailed methods are provided in the online version of this paper and include the following:

- KEY RESOURCES TABLE
- EXPERIMENTAL MODEL AND STUDY PARTICIPANT DETAILS
  - Clinical specimens
  - Animals
  - Cell lines and culture
- METHOD DETAILS
  - Mouse conventional DC1 generation and preparation
  - HER2 DC1 in combination with αSema4D therapy
  - BALB/c-HER2/neuT mice treatments
  - Human HER2-Bearing tumor model
  - CRISPR-mediated genetic ablation of Sema4D from TUBO and *in vivo* model of tumor-specific SEMA4D knockout
  - Cell-specific depletion and neutralizing treatments
  - IFN-γ KO mice model
  - 4T1 combination therapy
  - *Ex vivo* splenic CD4 T Cell Co-Culturing
  - *Ex vivo* experiment ELISA for IFN-γ expression
  - Multiplex immunofluorescence
  - Flow cytometry
  - Intracellular flow cytometry
  - NanoString sequencing
  - HER2 DC1 migration experiment
- QUANTIFICATION AND STATISTICAL ANALYSIS
  - Quantitative image analysis
  - Sema4D expression in human breast cancer patients
  - NanoString sequencing data analysis
  - Statistical analysis

SUPPLEMENTAL INFORMATION

Supplemental information can be found online at https://doi.org/10.1016/j.celrep.2026.117050.

Received: July 16, 2025
Revised: December 12, 2025
Accepted: February 5, 2026
Published: March 4, 2026

REFERENCES

1. Dhodapkar, M.V., Steinman, R.M., Sapp, M., Desai, H., Fossella, C., Krasovsky, J., Donahoe, S.M., Dunbar, P.R., Cerundolo, V., Nixon, D.F., and Bhardwaj, N. (1999). Rapid generation of broad T-cell immunity in humans after a single injection of mature dendritic cells. J. Clin. Investig. *104*, 173–180.
2. Cintolo, J.A., Datta, J., Mathew, S.J., and Czerniecki, B.J. (2012). Dendritic cell-based vaccines: barriers and opportunities. Future Oncol. *8*, 1273–1299.
3. Gautam, N., Elleson, K.M., Ramamoorthi, G., and Czerniecki, B.J. (2022). Current State of Cell Therapies for Breast Cancer. Cancer J. *28*, 301–309.
4. Gautam, N., Ramamoorthi, G., Champion, N., Han, H.S., and Czerniecki, B.J. (2024). Reviewing the significance of dendritic cell vaccines in interrupting breast cancer development. Mol. Aspects Med. *95*, 101239.
5. Wculek, S.K., Cueto, F.J., Mujal, A.M., Melero, I., Krummel, M.F., and Sancho, D. (2020). Dendritic cells in cancer immunology and immunotherapy. Nat. Rev. Immunol. *20*, 7–24.
6. Czerniecki, B.J., Roses, R.E., and Koski, G.K. (2007). Development of vaccines for high-risk ductal carcinoma in situ of the breast. Cancer Res. *67*, 6531–6534.
7. Lowenfeld, L., Mick, R., Datta, J., Xu, S., Fitzpatrick, E., Fisher, C.S., Fox, K.R., DeMichele, A., Zhang, P.J., Weinstein, S.P., et al. (2017). Dendritic Cell Vaccination Enhances Immune Responses and Induces Regression of HER2(pos) DCIS Independent of Route: Results of Randomized Selection Design Trial. Clin. Cancer Res. *23*, 2961–2971.
8. Sharma, A., Koldovsky, U., Xu, S., Mick, R., Roses, R., Fitzpatrick, E., Weinstein, S., Nisenbaum, H., Levine, B.L., Fox, K., et al. (2012). HER-2 pulsed dendritic cell vaccine can eliminate HER-2 expression and impact ductal carcinoma in situ. Cancer *118*, 4354–4362.
9. Basu, A., Albert, G.K., Awshah, S., Datta, J., Kodumudi, K.N., Gallen, C., Beyer, A., Smalley, K.S.M., Rodriguez, P.C., Duckett, D.R., et al. (2022). Identification of Immunogenic MHC Class II Human HER3 Peptides that Mediate Anti-HER3 CD4(+) Th1 Responses and Potential Use as a Cancer Vaccine. Cancer Immunol. Res. *10*, 108–125.
10. Ramamoorthi, G., Kodumudi, K., Snyder, C., Grover, P., Zhang, H., Greene, M.I., Basu, A., Gallen, C., Wiener, D., Costa, R.L.B., et al. (2022). Intratumoral delivery of dendritic cells plus anti-HER2 therapy triggers both robust systemic antitumor immunity and complete regression in HER2 mammary carcinoma. J. Immunother. Cancer *10*, e004841.
11. Ramamoorthi, G., Lee, M.C., Farrell, C.M., Snyder, C., Garg, S.K., Aldrich, A.L., Lok, V., Dominguez-Viqueira, W., Olson-Mcpeek, S.K., Rosa, M., et al. (2025). Antitumor CD4+ T helper 1 cells target and control the outgrowth of disseminated cancer cells. Cancer Immunol. Res. *13*, 729–748.
12. Han, H.S., Aldrich, A.L., Garg, S.K., Weinfurtner, R.J., Nguyen, J.V., Mo, Q., Whiting, J., Childress, J., Soliman, H., Costa, R., et al. (2025). Alteration of the Tumor Microenvironment With Intratumoral Dendritic Cells Before Chemotherapy in ERBB2 Breast Cancer: A Nonrandomized Clinical Trial. JAMA Oncol. *11*, 119–127.
13. Portera, C.C., Walshe, J.M., Rosing, D.R., Denduluri, N., Berman, A.W., Vatas, U., Velarde, M., Chow, C.K., Steinberg, S.M., Nguyen, D., et al. (2008). Cardiac toxicity and efficacy of trastuzumab combined with pertuzumab in patients with [corrected] human epidermal growth factor receptor 2-positive metastatic breast cancer. Clin. Cancer Res. *14*, 2710–2716.
14. Seidman, A., Hudis, C., Pierri, M.K., Shak, S., Paton, V., Ashby, M., Murphy, M., Stewart, S.J., and Keefe, D. (2002). Cardiac dysfunction in the trastuzumab clinical trials experience. J. Clin. Oncol. *20*, 1215–1221.

15. Durán-Gómez, N., López-Jurado, C.F., Nadal-Delgado, M., Pérez-Civantos, D., Guerrero-Martín, J., and Cáceres, M.C. (2022). Chemotherapy-Related Cognitive Impairment in Patients with Breast Cancer Based on Functional Assessment and NIRS Analysis. J. Clin. Med. *11*, 2363.

16. Kamgar, M., Greenwald, M.K., Assad, H., Hastert, T.A., McLaughlin, E.M., Reding, K.W., Paskett, E.D., Bea, J.W., Shadyab, A.H., Neuhouser, M.L., et al. (2021). Prevalence and predictors of peripheral neuropathy after breast cancer treatment. Cancer Med. *10*, 6666–6676.

17. Kang, D., Kim, I.R., Choi, E.K., Im, Y.H., Park, Y.H., Ahn, J.S., Lee, J.E., Nam, S.J., Lee, H.K., Park, J.H., et al. (2019). Permanent Chemotherapy-Induced Alopecia in Patients with Breast Cancer: A 3-Year Prospective Cohort Study. Oncologist *24*, 414–420.

18. Giaquinto, A.N., Sung, H., Newman, L.A., Freedman, R.A., Smith, R.A., Star, J., Jemal, A., and Siegel, R.L. (2024). Breast cancer statistics 2024. CA Cancer J. Clin. *74*, 477–495.

19. Sun, J., Zamyatnin, A.A., Jr., Yuan, X., Xiao, Y., and Li, H. (2023). Editorial: Cancer cell-intrinsic and -extrinsic factors affecting tumor immune evasion. Front. Immunol. *14*, 1261820.

20. Gurrapu, S., and Tamagnone, L. (2016). Transmembrane semaphorins: Multimodal signaling cues in development and cancer. Cell Adh. Migr. *10*, 675–691.

21. Hall, K.T., Boumsell, L., Schultze, J.L., Boussiotis, V.A., Dorfman, D.M., Cardoso, A.A., Bensussan, A., Nadler, L.M., and Freeman, G.J. (1996). Human CD100, a novel leukocyte semaphorin that promotes B-cell aggregation and differentiation. Proc. Natl. Acad. Sci. USA *93*, 11780–11785.

22. Ch'ng, E.S., and Kumanogoh, A. (2010). Roles of Sema4D and Plexin-B1 in tumor progression. Mol. Cancer *9*, 251.

23. Clavijo, P.E., Friedman, J., Robbins, Y., Moore, E.C., Smith, E., Zauderer, M., Evans, E.E., and Allen, C.T. (2019). Semaphorin4D Inhibition Improves Response to Immune-Checkpoint Blockade via Attenuation of MDSC Recruitment and Function. Cancer Immunol. Res. *7*, 282–291.

24. Sierra, J.R., Corso, S., Caione, L., Cepero, V., Conrotto, P., Cignetti, A., Piacibello, W., Kumanogoh, A., Kikutani, H., Comoglio, P.M., et al. (2008). Tumor angiogenesis and progression are enhanced by Sema4D produced by tumor-associated macrophages. J. Exp. Med. *205*, 1673–1685.

25. Evans, E.E., Jonason, A.S., Jr., Bussler, H., Torno, S., Veeraraghavan, J., Reilly, C., Doherty, M.A., Seils, J., Winter, L.A., Mallow, C., et al. (2015). Antibody Blockade of Semaphorin 4D Promotes Immune Infiltration into Tumor and Enhances Response to Other Immunomodulatory Therapies. Cancer Immunol. Res. *3*, 689–701.

26. Shafique, M.R., Fisher, T.L., Evans, E.E., Leonard, J.E., Pastore, D.R.E., Mallow, C.L., Smith, E., Mishra, V., Schröder, A., Chin, K.M., et al. (2021). A Phase Ib/II Study of Pepinemab in Combination with Avelumab in Advanced Non-Small Cell Lung Cancer. Clin. Cancer Res. *27*, 3630–3640.

27. Basile, J.R., Castilho, R.M., Williams, V.P., and Gutkind, J.S. (2006). Semaphorin 4D provides a link between axon guidance processes and tumor-induced angiogenesis. Proc. Natl. Acad. Sci. USA *103*, 9017–9022.

28. Prabhakaran, S., Rizk, V.T., Ma, Z., Cheng, C.H., Berglund, A.E., Coppola, D., Khalil, F., Mulé, J.J., and Soliman, H.H. (2017). Evaluation of invasive breast cancer samples using a 12-chemokine gene expression score: correlation with clinical outcomes. Breast Cancer Res. *19*, 71.

29. Wakil, A.E., Wang, Z.E., Ryan, J.C., Fowell, D.J., and Locksley, R.M. (1998). Interferon gamma derived from CD4(+) T cells is sufficient to mediate T helper cell type 1 development. J. Exp. Med. *188*, 1651–1656.

30. Jia, Y., Kodumudi, K.N., Ramamoorthi, G., Basu, A., Snyder, C., Wiener, D., Pilon-Thomas, S., Grover, P., Zhang, H., Greene, M.I., et al. (2021). Th1 cytokine interferon gamma improves response in HER2 breast cancer by modulating the ubiquitin proteasomal pathway. Mol. Ther. *29*, 1541–1556.

31. Denkert, C., von Minckwitz, G., Darb-Esfahani, S., Lederer, B., Heppner, B.I., Weber, K.E., Budczies, J., Huober, J., Klauschen, F., Furlanetto, J., et al. (2018). Tumour-infiltrating lymphocytes and prognosis in different subtypes of breast cancer: a pooled analysis of 3771 patients treated with neoadjuvant therapy. Lancet Oncol. *19*, 40–50.

32. Li, Y., Yang, X., Sun, Y., Li, Z., Yang, W., Ju, B., Easton, J., Pei, D., Cheng, C., Lee, S., et al. (2022). Impact of T-cell immunity on chemotherapy response in childhood acute lymphoblastic leukemia. Blood *140*, 1507–1521.

33. Zhang, Y., Yu, M., Jing, Y., Cheng, J., Zhang, C., Cheng, L., Lu, H., Cai, M.C., Wu, J., Wang, W., et al. (2021). Baseline immunity and impact of chemotherapy on immune microenvironment in cervical cancer. Br. J. Cancer *124*, 414–424.

34. Li, K., Shi, H., Zhang, B., Ou, X., Ma, Q., Chen, Y., Shu, P., Li, D., and Wang, Y. (2021). Myeloid-derived suppressor cells as immunosuppressive regulators and therapeutic targets in cancer. Signal Transduct. Target. Ther. *6*, 362.

35. Ozbay Kurt, F.G., Lasser, S., Arkhypov, I., Utikal, J., and Umansky, V. (2023). Enhancing immunotherapy response in melanoma: myeloid-derived suppressor cells as a therapeutic target. J. Clin. Investig. *133*, e170762.

36. Lu, J., Luo, Y., Rao, D., Wang, T., Lei, Z., Chen, X., Zhang, B., Li, Y., Liu, B., Xia, L., and Huang, W. (2024). Myeloid-derived suppressor cells in cancer: therapeutic targets to overcome tumor immune evasion. Exp. Hematol. Oncol. *13*, 39.

37. Mantovani, A., Allavena, P., Marchesi, F., and Garlanda, C. (2022). Macrophages as tools and targets in cancer therapy. Nat. Rev. Drug Discov. *21*, 799–820.

38. Jiang, H., Chen, C., Sun, Q., Wu, J., Qiu, L., Gao, C., Liu, W., Yang, J., Jun, N., and Dong, J. (2016). The role of semaphorin 4D in tumor development and angiogenesis in human breast cancer. OncoTargets Ther. *9*, 5737–5750.

39. Younis, R.H., Han, K.L., and Webb, T.J. (2016). Human Head and Neck Squamous Cell Carcinoma-Associated Semaphorin 4D Induces Expansion of Myeloid-Derived Suppressor Cells. J. Immunol. *196*, 1419–1429.

40. De Cicco, P., Ercolano, G., and Ianaro, A. (2020). The New Era of Cancer Immunotherapy: Targeting Myeloid-Derived Suppressor Cells to Overcome Immune Evasion. Front. Immunol. *11*, 1680.

41. Safarzadeh, E., Hashemzadeh, S., Duijf, P.H.G., Mansoori, B., Khaze, V., Mohammadi, A., Kazemi, T., Yousefi, M., Asadi, M., Mohammadi, H., et al. (2019). Circulating myeloid-derived suppressor cells: An independent prognostic factor in patients with breast cancer. J. Cell. Physiol. *234*, 3515–3525.

42. Speigl, L., Burow, H., Bailur, J.K., Janssen, N., Walter, C.B., Pawelec, G., and Shipp, C. (2018). CD14+ HLA-DR-/low MDSCs are elevated in the periphery of early-stage breast cancer patients and suppress autologous T cell proliferation. Breast Cancer Res. Treat. *168*, 401–411.

43. Itano, A.A., McSorley, S.J., Reinhardt, R.L., Ehst, B.D., Ingulli, E., Rudensky, A.Y., and Jenkins, M.K. (2003). Distinct dendritic cell populations sequentially present antigen to CD4 T cells and stimulate different aspects of cell-mediated immunity. Immunity *19*, 47–57.

44. Welsh, R.A., Song, N., and Sadegh-Nasseri, S. (2021). How Does B Cell Antigen Presentation Affect Memory CD4 T Cell Differentiation and Longevity? Front. Immunol. *12*, 677036.

45. Bennett, S.R., Carbone, F.R., Karamalis, F., Flavell, R.A., Miller, J.F., and Heath, W.R. (1998). Help for cytotoxic-T-cell responses is mediated by CD40 signalling. Nature *393*, 478–480.

46. Ridge, J.P., Di Rosa, F., and Matzinger, P. (1998). A conditioned dendritic cell can be a temporal bridge between a CD4+ T-helper and a T-killer cell. Nature *393*, 474–478.

47. Schoenberger, S.P., Toes, R.E., van der Voort, E.I., Offringa, R., and Melief, C.J. (1998). T-cell help for cytotoxic T lymphocytes is mediated by CD40-CD40L interactions. Nature *393*, 480–483.

48. Kumanogoh, A. (2002). [Involvement of immune semaphorins in the immune system]. Tanpakushitsu Kakusan Koso *47*, 2254–2260.

49. Suzuki, K., Kumanogoh, A., and Kikutani, H. (2008). Semaphorins and their receptors in immune cell interactions. Nat. Immunol. *9*, 17–23.

50. Goc, J., Germain, C., Vo-Bourgais, T.K.D., Lupo, A., Klein, C., Knockaert, S., de Chaisemartin, L., Ouakrim, H., Becht, E., Alifano, M., et al. (2014). Dendritic cells in tumor-associated tertiary lymphoid structures signal a Th1 cytotoxic immune contexture and license the positive prognostic value of infiltrating CD8+ T cells. Cancer Res. *74*, 705–715.

51. J Gunderson, A., Rajamanickam, V., Bui, C., Bernard, B., Pucilowska, J., Ballesteros-Merino, C., Schmidt, M., McCarty, K., Philips, M., Piening, B., et al. (2021). Germinal center reactions in tertiary lymphoid structures associate with neoantigen burden, humoral immunity and long-term survivorship in pancreatic cancer. OncoImmunology *10*, 1900635.

52. Cabrita, R., Lauss, M., Sanna, A., Donia, M., Skaarup Larsen, M., Mitra, S., Johansson, I., Phung, B., Harbst, K., Vallon-Christersson, J., et al. (2020). Tertiary lymphoid structures improve immunotherapy and survival in melanoma. Nature *577*, 561–565.

53. Lee, M., Heo, S.H., Song, I.H., Rajayi, H., Park, H.S., Park, I.A., Kim, Y.A., Lee, H., Gong, G., and Lee, H.J. (2019). Presence of tertiary lymphoid structures determines the level of tumor-infiltrating lymphocytes in primary breast cancer and metastasis. Mod. Pathol. *32*, 70–80.

54. Schumacher, T.N., and Thommen, D.S. (2022). Tertiary lymphoid structures in cancer. Science *375*, eabf9419.

55. Petroni, G., Pillozzi, S., and Antonuzzo, L. (2024). Exploiting Tertiary Lymphoid Structures to Stimulate Antitumor Immunity and Improve Immunotherapy Efficacy. Cancer Res. *84*, 1199–1209.

56. Hiam-Galvez, K.J., Allen, B.M., and Spitzer, M.H. (2021). Systemic immunity in cancer. Nat. Rev. Cancer *21*, 345–359.

57. Lazear, H.M., Nice, T.J., and Diamond, M.S. (2015). Interferon-lambda: Immune Functions at Barrier Surfaces and Beyond. Immunity *43*, 15–28.

58. Parker, B.S., Rautela, J., and Hertzog, P.J. (2016). Antitumour actions of interferons: implications for cancer therapy. Nat. Rev. Cancer *16*, 131–144.

59. Platanias, L.C. (2005). Mechanisms of type-I- and type-II-interferon-mediated signalling. Nat. Rev. Immunol. *5*, 375–386.

60. Beatty, G., and Paterson, Y. (2001). IFN-gamma-dependent inhibition of tumor angiogenesis by tumor-infiltrating CD4+ T cells requires tumor responsiveness to IFN-gamma. J. Immunol. *166*, 2276–2282.

61. Boulch, M., Cazaux, M., Cuffel, A., Guerin, M.V., Garcia, Z., Alonso, R., Lemaître, F., Beer, A., Corre, B., Menger, L., et al. (2023). Tumor-intrinsic sensitivity to the pro-apoptotic effects of IFN-gamma is a major determinant of CD4(+) CAR T-cell antitumor activity. Nat. Cancer *4*, 968–983.

62. Pepper, M., and Jenkins, M.K. (2011). Origins of CD4(+) effector and central memory T cells. Nat. Immunol. *12*, 467–471.

63. Zhang, H., Zhu, Z., Modrak, S., and Little, A. (2022). Tissue-Resident Memory CD4(+) T Cells Play a Dominant Role in the Initiation of Antitumor Immunity. J. Immunol. *208*, 2837–2846.

64. Godfrey, D.I., MacDonald, H.R., Kronenberg, M., Smyth, M.J., and Van Kaer, L. (2004). NKT cells: what's in a name? Nat. Rev. Immunol. *4*, 231–237.

65. Liu, X., Li, L., Si, F., Huang, L., Zhao, Y., Zhang, C., Hoft, D.F., and Peng, G. (2021). NK and NKT cells have distinct properties and functions in cancer. Oncogene *40*, 4521–4537.

66. Carreno, L.J., Saavedra-Avila, N.A., and Porcelli, S.A. (2016). Synthetic glycolipid activators of natural killer T cells as immunotherapeutic agents. Clin Transl Immunology *5*, e69.

67. King, L.A., Lameris, R., de Gruijl, T.D., and van der Vliet, H.J. (2018). CD1d-Invariant Natural Killer T Cell-Based Cancer Immunotherapy: alpha-Galactosylceramide and Beyond. Front. Immunol. *9*, 1519.

68. Molling, J.W., Kölgen, W., van der Vliet, H.J.J., Boomsma, M.F., Kruizenga, H., Smorenburg, C.H., Molenkamp, B.G., Langendijk, J.A., Leemans, C.R., von Blomberg, B.M.E., et al. (2005). Peripheral blood IFN-gamma-secreting Valpha24+Vbeta11+ NKT cell numbers are decreased in cancer patients independent of tumor type or tumor load. Int. J. Cancer *116*, 87–93.

69. Yoneda, K.i., Morii, T., Nieda, M., Tsukaguchi, N., Amano, I., Tanaka, H., Yagi, H., Narita, N., and Kimura, H. (2005). The peripheral blood Valpha24+ NKT cell numbers decrease in patients with haematopoietic malignancy. Leuk. Res. *29*, 147–152.

70. Campos, M., DE Campos, S.G.P., Ribeiro, G.G., Eguchi, F.C., Silva, S.R.M.D., DE Oliveira, C.Z., DA Costa, A.M., Curcelli, E.C., Nunes, M.C., Penna, V., and Longatto-Filho, A. (2013). Ki-67 and CD100 immunohistochemical expression is associated with local recurrence and poor prognosis in soft tissue sarcomas, respectively. Oncol. Lett. *5*, 1527–1535.

71. Kato, S., Kubota, K., Shimamura, T., Shinohara, Y., Kobayashi, N., Watanabe, S., Yoneda, M., Inamori, M., Nakamura, F., Ishiguro, H., et al. (2011). Semaphorin 4D, a lymphocyte semaphorin, enhances tumor cell motility through binding its receptor, plexinB1, in pancreatic cancer. Cancer Sci. *102*, 2029–2037.

72. Valente, G., Nicotra, G., Arrondini, M., Castino, R., Capparuccia, L., Prat, M., Kerim, S., Tamagnone, L., and Isidoro, C. (2009). Co-expression of plexin-B1 and Met in human breast and ovary tumours enhances the risk of progression. Cell. Oncol. *31*, 423–436.

73. Worzfeld, T., Swiercz, J.M., Looso, M., Straub, B.K., Sivaraj, K.K., and Offermanns, S. (2012). ErbB-2 signals through Plexin-B1 to promote breast cancer metastasis. J. Clin. Investig. *122*, 1296–1305.

74. Sun, Q., Zhou, H., Binmadi, N.O., and Basile, J.R. (2009). Hypoxia-inducible factor-1-mediated regulation of semaphorin 4D affects tumor growth and vascularity. J. Biol. Chem. *284*, 32066–32074.

75. Conrotto, P., Valdembri, D., Corso, S., Serini, G., Tamagnone, L., Comoglio, P.M., Bussolino, F., and Giordano, S. (2005). Sema4D induces angiogenesis through Met recruitment by Plexin B1. Blood *105*, 4321–4329.

76. Tamagnone, L., Artigiani, S., Chen, H., He, Z., Ming, G.I., Song, H., Chedotal, A., Winberg, M.L., Goodman, C.S., Poo, M., et al. (1999). Plexins are a large family of receptors for transmembrane, secreted, and GPI-anchored semaphorins in vertebrates. Cell *99*, 71–80.

77. Giordano, S., Corso, S., Conrotto, P., Artigiani, S., Gilestro, G., Barberis, D., Tamagnone, L., and Comoglio, P.M. (2002). The semaphorin 4D receptor controls invasive growth by coupling with Met. Nat. Cell Biol. *4*, 720–724.

78. Feigin, A., Evans, E.E., Fisher, T.L., Leonard, J.E., Smith, E.S., Reader, A., Mishra, V., Manber, R., Walters, K.A., Kowarski, L., et al. (2022). Pepinemab antibody blockade of SEMA4D in early Huntington's disease: a randomized, placebo-controlled, phase 2 trial. Nat. Med. *28*, 2183–2193.

79. Benitez, A., Weldon, A.J., Tatosyan, L., Velkuru, V., Lee, S., Milford, T.A., Francis, O.L., Hsu, S., Nazeri, K., Casiano, C.M., et al. (2014). Differences in mouse and human nonmemory B cell pools. J. Immunol. *192*, 4610–4619.

80. Korzhenevich, J., Janowska, I., van der Burg, M., and Rizzi, M. (2023). Human and mouse early B cell development: So similar but so different. Immunol. Lett. *261*, 1–12.

81. Zilionis, R., Engblom, C., Pfirschke, C., Savova, V., Zemmour, D., Saatcioglu, H.D., Krishnan, I., Maroni, G., Meyerovitz, C.V., Kerwin, C.M., et al. (2019). Single-Cell Transcriptomics of Human and Mouse Lung Cancers Reveals Conserved Myeloid Populations across Individuals and Species. Immunity *50*, 1317–1334.e10.

82. Ritchie, M.E., Phipson, B., Wu, D., Hu, Y., Law, C.W., Shi, W., and Smyth, G.K. (2015). limma powers differential expression analyses for RNA-sequencing and microarray studies. Nucleic Acids Res. *43*, e47.

STAR★METHODS

KEY RESOURCES TABLE

REAGENT or RESOURCE	SOURCE	IDENTIFIER
Antibodies		
Pepinimab: monoclonal anti-Semaphporin 4D (mab 67)	Vaccinex; Rochester, NY	https://doi.org/10.1080/13543784.2025.2473055
HER2/ErbB2 (29D8) Rabbit mAb	Cell Signaling	Cat. 2165S; RRID:AB_10692490
InVivoMAb anti-mouse CD4 (Clone GK1.5)	BioXCell	Cat. No. BE0003-1; RRID:AB_1107636\1
InVivoMab anti-mouse CD8α (Clone2.43)	BioXCell	Cat. No. BE0061: RRID:AB_1125541
Rat IgG2b isotype (Clone LTF-2)	BioXCell	Cat. No. BE0090; RRID:AB_1107780
InVivoPlus anti-mouse CD20 (Clone MB20-11)	BioXCell	Cat. No. BE0356; RRID:AB_2894775
InVivoPlus anti-mouse CD40 (clone MR-1)	BioXCell	Cat. No. BE0016-2; RRID:AB_1107647\1
Mouse anti-Cytokeratin 7	Fisher	Cat. No. BP1605
Fluorescein (FITC)-AffiniPure Goat Anti-Mouse IgG (H+L)	Fisher	Cat. No. 115-095-003; RRID:AB_2338589
Anti-Mouse CD45 BUV395 (Clone 30-F11)	BD Biosciences	Cat. No. 564279; RRID:AB_2651134
Anti-Mouse CD3 APC (Clone 145-2C11)	BD Biosciences	Cat. No. 553066; RRID:AB_398529
Anti-Mouse CD8 BV421 (Clone 53–6.7)	BD Biosciences	Cat. No. 563898; RRID:AB_2738474
Anti-Mouse CD4 BB700 (Clone RM4-5)	BD Biosciences	Cat. No. 566407; RRID:AB_2744427
Anti-Mouse CD62L BUV737 (Clone MEL-14)	BD Biosciences	Cat. No. 612833; RRID:AB_2870155
Anti-Mouse CD44 FITC (Clone IM7)	BD Biosciences	Cat. No. 553133; RRID:AB_2076224
Anti-Mouse CD49b PE (Clone DX5)	BioLegend	Cat. No. 108908; RRID:AB_313415
Anti-Mouse CD19 PE/Cyanine7 (Clone 6D5)	BioLegend	Cat. No. 115520; RRID:AB_313655
Anti-Mouse CD45 BUV395 (Clone 30-F11)	BD Biosciences	Cat. No. 564279; RRID:AB_2651134
Anti-Mouse CD11b PerCP-Cy5.5 (Clone M1/70)	BD Biosciences	Cat. No. 550993; RRID:AB_394002
Anti-Mouse GR1 APC (Clone RB6-8C5)	BD Biosciences	Cat. No. 553129; RRID:AB_398532
Anti-Mouse aCD11c PE (Clone N418)	BioLegend	Cat. No. 117308; RRID:AB_313777
Anti-Mouse CD80 BV421 (Clone 16-10A1)	BioLegend	Cat. No. 104725; RRID:AB_10900989
Anti-Mouse F4/80 PE/Cyanine7 (Clone BM8)	BioLegend	Cat. No. 123114; RRID:AB_893478
Anti-Mouse CD206 BV650 (Clone C086C2)	BioLegend	Cat. No. 141723; RRID:AB_2562445
Anti-Mouse Tbet AF594 (Clone 4B10)	BioLegend	Cat. No. 644834; RRID:AB_2728474
Anti-Mouse Interferon gamma BV650 (Clone XMG1.2)	BD Biosciences	Cat. No. 554412; RRID:AB_395376
Anti-Mouse CD45 FITC (Clone 30-F11)	Fisher	Cat. No. 11-0451-82; RRID:AB_465050
Anti-Mouse CD11c BV785 (Clone N418)	BioLegend	Cat. No. 117336; RRID:AB_2565268
Chemicals, peptides, and recombinant proteins		
HER2/Neu P (5ELAAWCRWGFLLALLPPGIAG)	Bachem Holding AG	Cat. No. 4108540

(*Continued on next page*)

Continued

REAGENT or RESOURCE	SOURCE	IDENTIFIER
HER2/Neu P435 (IRGRILHDGAYSLTLQGLGIH)	Bachem Holding AG	Cat. No. 4108541
HER2/Neu P1209 (SPPHPSPAFSPAFDNLYYWDQ)	Bachem Holding AG	Cat. No. 4108542
HER3 ECD Class II peptides (p12, p81, p84, p91)	Genscript	N/A
HER3 ICD Class II peptides (p38, p41, p52, p86, p89)	Genscript	N/A
Mouse IL-4	R&D	Cat. No. 404-ML-050
Mouse GM-CSF	R&D	Cat. No. 415-ML-050
ODN1896	Fisher	Cat. No. NC9685794
Lipopolysaccharide	Signma-Aldrich	Cat. No. L4391-1MG
RPMI-1640 media	Corning	Cat. No. 10-040-CM
Fetal bovine serum	Corning	Cat. No. 35-015-CV
sodium pyruvate	Fisher Scientific	Cat. No. MT-25-000-CI
L-Glutamine	Fisher	Cat. No. 25005CI
Penicillin/Streptomycin	Corning	MT-30-002-CI
Gentamycin	Fisher	Cat. No. BW17-519Z
Fungizone	Life Technologies	Cat. No. 17-836E
2-Mercaptoethanol	Sigma-Aldrich	Cat. No. M3148
nonessential amino acids	Corning	Cat. No. 25-025-CI
Critical commercial assays		
EasySep $CD4^+$ T Cell Isolation Kit	Stemcell	Cat. No. 19852
PerkinElmer OPAL 7-Color Automation IHC Kit	Leica Biosystems	Cat. No. OP-000003
Mouse IFN gamma ELISA Quantikine kit	R&D	Cat. No. SMIF00
PanCancer IO 360™ RNASeq Panel	NanoString Technologies	Cat. No. LBL-10545-01
Metabolic Pathways RNASeq Panel	NanoString Technologies	Cat. No. LBL-10726-01
Myeloid Innate Immunity RNASeq Panel	NanoString Technologies	Cat. No. LBL-10398-02
Immunology RNASeq Panel	NanoString Technologies	Cat. No. LBL-C0268-02
P3 Primary Cell 4D-Nucleofector® X Kit S	Lonza Bioscience	Cat. No. V4XP-3032
Deposited data		
NanoString PanCancer Panel Raw Data from this lab	This study	GEO: GSE302765
NanoString Metabolic Pathways Panel Raw Data from this lab	This study	GEO: GSE302735
NanoString Myeloid Innate Immunity Panel Raw Data from this lab	This study	GEO: GSE302763
NanoString Immunology Panel Raw Data from this lab	This study	GEO: GSE302764
Experimental models: Cell lines		
Mouse: hHER2 CT26	William E. Carson Lab of Ohio State	https://doi.org/10.1158/1078-0432.CCR-09-2591.
Mouse:TUBO	Dr. Brian Czerniecki Lab	https://doi.org/10.1136/jitc-2022-004841
Mouse: 4T1	ATCC	Cat. No. CRL-2539 RRID: CVCL_0125
TUBO *Sema4D*$^{-/-}$	This study	N/A
Experimental models: Organisms/strains		
Mouse: Balb/c wild-type	Charles River	RRID: IMSR_CRL:028

(*Continued on next page*)

Continued

REAGENT or RESOURCE	SOURCE	IDENTIFIER
Mouse: BALB/c-HERNeuT	Shari Pilon-Thomas Lab, Moffitt Cancer Center	https://doi.org/10.4049/jimmunol.20004661
Mouse: C.129S7(B6)-Ifngtm1Ts/J	Jackson Laboratory	RRID:IMSR_JAX:002663\1
Mpouse: C57BL/6 wild-type	Charles River	RRID: IMSR_CRL:027\1
Recombinant DNA		
Mm.Cas9.SEMA4D.1.AA CAAGAACAGCCCCCTAACGG GGG(PAM)	IDT	N/A
Mm.Cas9.SEMA4D.1.AB. GAAGACGAATTCGTACTCCA CGG(PAM)	IDT	N/A
Alt-R™ S.p. Cas9 Nuclease V3	IDT	Cat# 1081058
Alt-R™ Cas9 Negative Control crRNA #1	IDT	Cat# 1072544
Alt-R™ CRISPR-Cas9 tracrRNA	IDT	Cat# 1072532
Software and algorithms		
Vectra3 Automated Quantitative Pathology Imaging System	Moffitt Cancer Center SAIL Core Facility	RRID:SCR_025828
ImageJ	NIH	RRID:SCR_003070
HALO Image Analysis Platform version 3.6.4134	Indica Labs	RRID:SCR_018350
Graphpad Prism version 10	Graphpad Software, LLC	RRID:SCR_002798
Genomic Data Commons Data Portal	GDC	RRID:SCR_014514
nSolver4.0TM software	Moffitt Cancer Center Bioinformatics Core Facility	RRID:SCR_003420
FCS express	*De Novo* Software	RRID:SCR_016431
Other		
7-Tesla horizontal MRI scanner	Moffitt Cancer Center SAIL Core Facility	RRID:SCR_012401
Cellaca MX	Nexcelom	RRID: MX-AOPI
K2 Cellometer	Nexcelom	RRID: CHT4-SD100-014
BioTek Synergy H1 Multimode Reader	Agilent	RRID:SCR_019748
BD LSR II Flow Cytometer	BD Bioscience	RRID:SCR_002159
BD Symphony A5 Flow Cytometer	BD Bioscience	RRID:SCR_022538

EXPERIMENTAL MODEL AND STUDY PARTICIPANT DETAILS

Clinical specimens

Tumor tissue microarray analysis of SEMA4D expression by immunofluorescence from 90 Triple-negative breast cancer patients was obtained from samples collected in the retrospective study reviewed and approved by the Institutional Review Board at the H. Lee Moffitt Cancer Center and Research Institute (protocol ID: MCC20581). Tumor needle biopsies for immunofluorescence analysis of SEMA4D expression were obtained from 15 HER2-positive breast cancer patients enrolled in the clinical trial NCT03387553 at the H. Lee Moffitt Cancer Center and Research Institute.

Animals

Due to the majority of cases of breast cancer among the female population, we conducted our studies on female mouse models representing the appropriate sex for examination of therapy-related effects. Female BALB/c mice (6-8 weeks) were purchased from Charles River (Wilmington, MA), Female C.129S7(B6)-Ifngtm1Ts/J (IFN-γ KO) mice were obtained from The Jackson Laboratory (Bar Harbor, ME), BALB/c-HER2/neuT transgenic mice were a kind gift from Dr. Shari Pilon-Thomas (H. Lee Moffitt Cancer Center & Research Institute). All mice were housed in the Animal Research Facility of the H. Lee Moffitt Cancer Center. The mice were kept in individually ventilated cages in housing rooms maintained at 20-24°C, on a 12-hour light/dark cycle with lights off at 6:00 pm. Litters of a maximum of 5 mice per cage, of the same sex, were used for post-weaning treatment groups involving 6-10 mice; two cages per

group were used. Cage food and water were monitored daily and refilled weekly, with cages and water bottles swapped and autoclaved every other week. The study protocol was designed in accordance with the guidelines outlined in the Guide for the Care and Use of Laboratory Animals of the National Institutes of Health. The Institutional Animal Care and Use Committee approved the protocol at the University of South Florida (#A4100-01). Animals were monitored daily by research facility staff, and lab members were notified of any health concerns occurring during *in vivo* models. For each murine model, approximately 6-8 mice per treatment group were used, as the minimum sample size needed to detect a statistically significant difference arising from an effective response to combinational therapy and to minimize suffering. Mice were humanely euthanized when necessary, using CO_2 inhalation followed by cervical dislocation, at the end of the study or when tumor size exceeded the endpoint. Ulceration on the tumor is limited to an area less than 5x5 mm on the tumor's surface; anything larger is considered an endpoint, and the mice are euthanized regardless of tumor size. This follows the American Veterinary Medical Association Guidelines to ensure minimal suffering.

Cell lines and culture

TUBO, a mouse mammary carcinoma cell line (a gift from Dr. Wei Zen Wei, Wayne State University), was cloned from spontaneous mammary tumors in BALB-HER2/neu transgenic mice. Human HER2-expressing (hHER2) CT26 cell line was kindly provided by Dr. William E. Carson (The Ohio State University). 4T1, a triple-negative breast cancer cell lines was purchased from ATCC (CRL-2539, RRID: CVCL_0125). Cell lines were tested for mycoplasma upon first receiving in the lab and upon culture, as well as when stock expansion was necessary. All cell lines in the lab have been confirmed to be mycoplasma negative. The cell lines were not authenticated by STR profiling, but they were passed through mice prior to testing and used in all experiments within 6 passages, with growth rate and viability monitored thoroughly before use. Cells were cultured in complete medium: RPMI-1640 media (Corning, NY; Cat. No. 10-040-CM) supplemented with 10% heat-inactivated fetal bovine serum (FBS, Corning, NY; Cat. No. 35-015-CV), 0.1 mM nonessential amino acids (Corning, Corning, NY; Cat. No. 25-025-CI), 1.0 mM sodium pyruvate (Fisher Scientific, Waltham, MA; Cat. No. MT-25-000-CI), 2.0 mM L-glutamine (Fisher; Cat. No. 25005CI), 100 mg/ml streptomycin (Corning; Cat. No. MT-30-002-CI), 100 U/ml penicillin (Corning; Cat. No. MT-30-002-CI), 50 mg/mL gentamycin (Fisher; Cat. No. BW17-519Z), 0.5 mg/mL fungizone (Life Technologies; Cat. No. 17-836E) and 0.05 mM 2-Mercaptoethanol (Sigma Aldrich, St. Louis, MO; Cat. No. M3148). Cells were cultured in a 5% CO_2 incubator, kept at 37°C, and grown to at least 80% of confluency.

METHOD DETAILS

Mouse conventional DC1 generation and preparation

Immature DCs were processed from naïve female BALB/c mice aged 6-8 weeks as previously described.[9] For cDC1 preparation, immature DCs were plated at $2e^6$ cells/ml in complete medium spiked with 50 ng/ml GM-CSF (R&D Systems, Minneapolis, MN; Cat. No. 415-ML-050) and 10 ng/ml IL-4 (R&D; Cat. No. 404-ML-050) and incubated in 5% CO_2 incubator at 37°C overnight. The multi-epitope MHC class II HER2/Neu peptides p5, p435, and p1209 (custom-made by Bachem Holding AG, Bubendorf, Switzerland; cat. nos. 4108540, 4108541, 4108542) were added to separate flasks at a concentration of 10 μg/ml to ensure uniform specificity between each peptide. TLR agonists CPG at 10 ng/ml (Fisher; Cat. No. NC9685794) and LPS at 20 ng/ml (Sigma Aldrich; Cat. No. L4391-1MG) were added 4-6 hours after peptides for DC1 polarization, then cells were incubated overnight. On the day of treatment, the peptide-pulsed DC1 cells were pooled with their respective peptide groupings, washed with PBS, and injected intratumorally at 1 × 10^6 cells/50 μL per mouse.

HER2 DC1 in combination with αSema4D therapy

TUBO cells ($2.5e^5$ cells/mouse) were injected subcutaneously on the left flank of naïve female BALB/c mice at weeks 8-10 for the subcutaneous tumor model. TUBO cells (3 × 10^4 cells/mouse) were injected into the mammary fat pad to establish an orthotopic tumor model. Mice were pooled and randomized once tumor palpability was measurable, and prior to initial treatments, assigning 6-8 mice per treatment group, including an untreated control. The monotherapy groups received either HER2 DC1 (1 × 10^6 cells/mouse; intratumoral delivery) or αSema4D (Mab67, Vaccinex Inc., Rochester, NY) (10 mg/kg; intraperitoneal) once weekly for six weeks. The combination therapy group received two injections of αSema4D (10 mg/kg; intraperitoneally) in week one. They then continued with HER2 DC1 in combination with αSema4D weekly for six weeks. In some experiments, tumor-bearing mice were also treated with HER2 DC1 subcutaneous delivery alone, immature HER2 DC1 intratumoral delivery alone, or in combination with αSema4D antibody. Tumors were measured using calipers for the length × width area. Endpoint tumor size for subcutaneous TUBO tumors was 400 mm^2, or until tumor ulceration reached 25 mm^2, at which point mice were humanely euthanized. Orthotopic tumors were measured using the tumor volume calculation [tumor volume (mm^3) = (length x $width^2$)/2], and the endpoint was determined to be 3000 mm^3 volume. For high tumor burden models, treatment was delayed until the tumors reached an area of approximately 75-100 mm^2. Bilateral tumor models involved two subcutaneous TUBO injections on either flank of the mice, and HER2 DC1 intratumoral injections were performed solely on the left flank tumor, with distant tumors being left untreated. To maintain a consistent endpoint tumor burden, the mice were euthanized once the cumulative tumor size between both tumors reached 400 mm^2 or when one of the tumors reached 250 mm^2.

BALB/c-HER2/neuT mice treatments

Female BALB/c-HER2/neuT mice at 11 weeks old were treated with intratumoral HER2 DC1 alone, anti-SEMA4D antibody alone, or a combination of both as described above. Magnetic resonance imaging (MRI) was performed at various time points in the experimental mice to examine the spontaneous development of mammary carcinoma in all ten mammary glands, as previously described.[10] Briefly, experimental mice were anesthetized in an induction chamber using 2% isoflurane with an oxygen supply of 1.5 liters per minute. The 7-Tesla horizontal MRI scanner (Bruker Biospin, Inc., Billerica, MA, BioSpec AV3HD) equipped with a 35 mm Litzcage coil (Doty Scientific, Columbia, SC) was used for the imaging. The anesthetized mice were placed in the MRI scanner, and continuous ventilation was provided via a nose cone. The respiration range was maintained between 40 and 60 breaths per minute throughout the imaging. The body temperature was maintained at 37°C with the aid of an MR-compatible Small Rodent Heater System (SAII, SA Instruments, Stony Brook, NY). The anatomical T2-weighted coronal images with specifications of slice thickness 1.2 mm/19 slices, field of view (FOV) = 75 x 35 $mm^{2,}$ and echo time/repetition time (TR/TE) = 4513/38 ms were taken with the help of TurboRARE sequence.

Human HER2-Bearing tumor model

The three mouse HER2 peptides used in DC1 antigen presentation were found to be at least 90% homologous with human HER2 expression, so it was important to test that in an *in vivo* model. Human HER2-expressing (hHER2) CT26 cell line provided by Dr. William E. Carson (The Ohio State University) were placed into female BALB/c mice at age 8-10 weeks and were subcutaneously injected (3 × 10^5 cells/mouse). After the establishment of palpable tumors, mice were pooled, randomized into groups of eight mice each, treated with HER2 DC1 or anti-Sema4D antibody every five days. For combination therapy, mice received two injections of anti-Sema4D antibody in the first week. Then, mice received HER2 DC1 concurrently with anti-Sema4D. Tumor size was measured twice a week. For CT26 models, the endpoint tumor volume for subcutaneous tumors was set at 350 mm^2.

CRISPR-mediated genetic ablation of Sema4D from TUBO and *in vivo* model of tumor-specific SEMA4D knockout

Anti-Sema4d predesigned Alt-R CRISPR-Cas9 gRNA (200 μM, Mm.Cas9.SEMA4D.1.AB, IDT) or negative control (200 μM, Cat#1072544, IDT) was equimolarly combined with tracrRNA (200 μM, Cat#1072532, IDT) and incubated at 95°C for 5 minutes. SpCas9 V3 (62 μM, Cat#1081058, IDT) was added to the duplex after 15 minutes and incubated for 29 minutes at room temperature. The RNP complex was combined with 5 × 10^6 TUBO cells and electroporated using the P3 Primary Cell (Cat# V4XP-3024) protocol and the EN-130 program from Amaxa 4D Nucleofector. After electroporation, the TUBO cells were expanded with RPMI + 10% FBS media for 5 days. TUBO Sema4D$^{-/-}$ were stained with DAPI and anti-mouse SEMA4D-PE (Cat#147603, Biolegend) for cell sorting using MACSQuant Tyto Cell sorter. The efficiency of knockout was evaluated by flow cytometry on TUBO crNTC or Sema4D$^{-/-}$ cells using anti-mouse SEMA4D-PE or isotype control (Cat#400507, Biolegend).

Secondary confirmation of the knockout was conducted by immunofluorescence staining on the cell line, marking Sema4D expression using anti-goat FITC (Fisher; Cat. No. 115-095-003) and DAPI mounting medium (Vector Laboratories). Images were taken on the X-B810 fluorescent microscope (Keyence, Itasca, Illinois). Histograms for pixel intensity measurements in the Sema4D channel for *Sema4D*$^{+/+}$ and *Sema4D*$^{-/-}$ TUBO were generated using ImageJ. A comparison of the combinational therapy was conducted in female BALB/c mice using the *Sema4D*$^{+/+}$ versus *Sema4D*$^{-/-}$ TUBO cell line. Using fifty-five mice in total, Twenty-seven mice for each tumor cell line were injected subcutaneously with 2.5e5 TUBO cells in 100 μL of PBS. By Day 7, palpable tumors were present in all mice from both the wild-type and knockout cohorts, and our standard combination approach began, with 6-7 mice per group. Weekly doses of anti-Sema4D and HER2-pulsed DC1, as previously mentioned, were administered for 6 weeks, while the tumor area was monitored twice weekly, and the mice were assessed for endpoint criteria. The CRISPR cell line model was directly compared to the wild-type model.

Cell-specific depletion and neutralizing treatments

Each Depletion model below was used to explore the role of a single immune cell population on how the combinational therapy functions against the HER2-positive tumor in naive female BALB/c mice aged 8-10 weeks.

CD4 and CD8 T cell depletion

Thirty Female naïve BALB/c mice were injected intraperitoneally with 300 μg of anti-CD4 (clone GK1.5 purchased from BioXCell, Lebanon, NH; Cat. No. BE0003-1) or anti-CD8 (clone 2.43, BioXCell; Cat No. BE0061) antibodies three days prior to TUBO injection. The $CD4^+$ and $CD8^+$ T cell depletion antibodies were administered twice a week until the experimental endpoints to maintain the proper lack of the targeted immune cell populations. The non-depleted control group received an intraperitoneal injection of rat IgG2b isotype antibody at the same intervals as the depletion groups. Treatments were given as described above. For the CD4 T cells early depletion experiment, mice received anti-CD4 injections until three monotherapies or three combination therapies were completed. For the CD4 T cell late depletion experiment, mice received anti-CD4 injections starting from the fourth monotherapy or fourth combination therapy and continued until the completion of all six monotherapies or combination therapies.

B cell depletion

Twenty-five female naïve BALB/c mice were randomized into two pools, one pool was depleted of B cells one day prior to tumor injection. The mice were injected intraperitoneally with 250 μg of αCD20 monoclonal antibody (BioXCell, clone MB20-11; Cat. No. BE0356). The Mice were injected the following day with 2.5 × 10^5 TUBO cells subcutaneously. Once palpable, mice were treated

with HER2 DC1 intratumorally and αSema4D intraperitoneally as described previously. The treatment groups were duplicated in both naïve BALB/c mice and the depleted BALB/c mice for comparison and were measured twice/week until the endpoint.

CD40L blocking

Repeating the TUBO subcutaneous model, the importance of CD40L during T cell-DC1 interaction was put to the test using a CD40L blocking agent (BioXCell, Clone MR-1; Cat. No. BE0017-1) given at 10 mg/kg weekly. HER2 DC1 and αSema4D treatment was given as previously described for other models, using. The tumor endpoint was measured twice weekly to determine if the combinational therapy works while CD40L is inhibited.

IFN-γ KO mice model

Female C.129S7(B6)-Ifngtm1Ts/J (IFN-γ KO) mice were obtained from The Jackson Laboratory at 8-10 weeks old, for investigating the dependency of the primary function of CD4 T helper cells, influenced by the combination therapy to combat tumor growth. 2.5e6 TUBO cells were injected into the left flank or 25 mice and then treated with either HER2 DC1, αSema4D antibody, or a combination of both on a weekly basis, as reflected in the above *in vivo* models Tumor growth was monitored and measured twice a week until endpoint size of 400mm^2 was reached.

4T1 combination therapy

Interest in expanding the effective DC1 and Sema4D antibody in multiple breast cancer types led to a study of triple-negative breast cancer involving the 4T1 cell line. 20 Female BALB/c mice at age 8-10 weeks were injected subcutaneously with 3e^5 4T1 cells on the left flank. Tumors were quickly palpable at 3 days post tumor injections, and mice were randomized into groups of 6 to either receive no treatment, HER3 DC1, or HER3 DC1 and Sema4D antibody. Treatment was given twice weekly in this model due to the rapidity of tumor growth and lung metastasis in the 4T1 cell line in mice. The animals were monitored until endpoint criteria of either a tumor size of 250mm^2, ulceration on the tumor surface, or signs of declining health due to metastasis, at which point the mice were euthanized.

Ex vivo splenic CD4 T Cell Co-Culturing

Spleens isolated from various the four therapy groups of our *in vivo mouse models* were dissociated and stored in PBS into suspension cell solutions and lysed of red blood cells using an ACK lysis buffer produced in lab. The remaining splenocytes were isolated using the CD4$^+$ T cell EasySep isolation kit (Stemcell Technologies; Cat. No. 19852). Cells were resuspended at a concentration of 1 × 10ˆ8 cells/mL in PBS and incubated with the antibody cocktail for 10 minutes at room temperature. CD4$^+$ T cells were isolated from splenocytes as described in the manufacturer's protocol. Isolated cells were placed in a polypropylene tube before being counted on the Cellaca MX cellometer (Nexelom), this was the working splenic CD4$^+$ T cell population. The T cells were plated into a 24-well plate, with 1 × 10ˆ6 cells per well in 2 mL of CM. Isolated CD4$^+$ T cells were co-cultured with HER2 pulse DC1 at a 10:1 ratio. The coculture was incubated at 37°C for 24 hours, at which point the supernatant was collected and used for an interferon gamma ELISA assay. Protein transportation was inhibited in the co-cultured T cells via protein transport inhibitor cocktail (Invitrogen; Cat. No. 00-4980-93) for 4 hours prior to harvesting, and the cells were used in the intracellular staining procedure seen below, including mouse anti-Interferon-γ BV650 (BD Bioscience, clone XMG1.2: Cat. No. 554412) and anti-T-bet AF594 (Biolegend, clone 4B10: Cat. No. 644834) as described in the intracellular flow staining method.

Ex vivo experiment ELISA for IFN-γ expression

Supernatants from mouse splenocytes cocultured with HER2 DC1 were analyzed by IFN-γ ELISA assay kit (R&D; Cat. No. SMIF00). Samples were run in triplicate with 50 μL of supernatant per well in a 96-well precoated plate, along with serially diluted standards supplied with the kit. The plate was washed three times with 250 μL of wash buffer per well after 2 hours of incubation at room temperature, and 100 μL of conjugated antibody buffer was added to each well for an additional 2 hours. A second wash was performed, followed by a final 30-minute incubation with 100 μL of color reagent. Afterward, the reaction was halted with 100 μL of stop solution. The assay was read on a Synergy H1 microplate reader (Fisher, BioTek Inc., Cat. No. 11-120-533).

Multiplex immunofluorescence

Sections of mouse tumor tissue, harvested from *in vivo* treatment models, were stained for Semaphorin 4D (Vaccinex) and Cytokeratin 7 (Ventana, Tucson, AZ; Cat. No. 790-4462). The sections were baked at 70°C vertically to remove the protective wax layer, and then soaked in several baths of xylene, followed by ethanol and water, with 1-5 min intervals between each bath. Tissues were then submerged in antigen-unmasking buffer (Vector Laboratories, Newark, CA; Cat. No. H-3300-250) and placed into a pressure cooker set to High for 15 minutes. Once cooled and rinsed in DI water, tissue sections were incubated in protein blocking solution (Vector Laboratories) for 2 hours, followed by an overnight 4°C incubation with a combined solution of primary antibodies of anti-Sema4D and anti-KRT7, diluted at 1:400 each in 5% Bovine serum albumin (Fisher; Cat. No. BP1605). The next day, tissues were washed with 1x PBS, followed by incubation with secondary antibodies in 5% BSA at a 1:400 dilution, and then incubated for 4 hours in the dark. Tissue sections were finally stained with 2-5 μL of DAPI blue mounting medium (Vector Laboratories) underneath a coverslip, which was sealed with clear nail polish. All samples were run on an X-B810 fluorescent microscope (Keyence, Itasca, Illinois).

Mouse tumor tissue blocks and human FFPE needle biopsies were immunostained using the PerkinElmer OPAL™ 7-Color Automation IHC kit (Waltham, MA) on the BOND RX autostainer (Leica Biosystems, Vista, CA). The OPAL 7-color kit uses tyramide signal

amplification (TSA), conjugated to individual fluorophores, to detect various targets within the multiplex assay. Sections were baked at 65°C for one hour and then transferred to the BOND RX (Leica Biosystems). All subsequent steps (e.g., deparaffinization and antigen retrieval) were performed using an automated OPAL IHC procedure (PerkinElmer, Waltham, MA). OPAL staining of each antigen was performed as follows: slides were blocked with PerkinElmer blocking buffer for 10 minutes, then incubated with primary antibody at optimized concentrations, followed by OPAL HRP polymer and one of the OPAL fluorophores. Individual antibody complexes are stripped after each round of antigen detection. After the final stripping step, the DAPI counterstain is applied to the multiplexed slide and is removed from BOND RX for coverslipping. Autofluorescence slides (negative control) were included, which use primary and secondary antibodies, omitting the OPAL fluors and DAPI. All slides were imaged using the Vectra®3 Automated Quantitative Pathology Imaging System.

Flow cytometry

Tumors were collected from the experimental mice. Tumor Digest solution was prepared using HBSS (Fisher; Cat. No. MT-21-022-CM), containing 1 mg/ml collagenase (Sigma Aldrich; Cat. No. C9891), 0.1 mg/ml DNase I (Sigma Aldrich; Cat. No. DN25), and 2.5U/ml of hyaluronidase (Sigma Aldrich; Cat. No. H-6254-1G). Minced tumors were incubated in tumor digest solution for 1 hour at 37°C in a water bath. Red blood cells were lysed using ACK lysis buffer for 5 min at room temperature. For analyzing the immune cell population within the tumors, single-cell suspensions were placed at $1e0^6$ cells into 5.0 ml FACS tubes and incubated with Live/Dead Zombie near IR (Biolegend, San Diego, CA; Cat. No. 423106) for 30 min in the dark at room temperature. Cells were then washed with FACS buffer and stained with a pooled solution of selected anti-mouse antibodies for lymphoid immune cells panel [anti-CD45 BUV 395 (BD Biosciences, San Jose, CA; Cat. No. 564279, Clone 30-F11), anti-CD3 APC (BD Biosciences, Clone 145-2C11; Cat. No. 553066), anti-CD8 BV421 (BD Biosciences, Clone 53–6.7; Cat. No. 563898), anti-CD4 BB700 (BD Biosciences, Clone RM4-5; Cat. No. 566408), anti-CD62L BUV737 (BD Biosciences, Clone MEL-14; Cat. No. 612833), anti-CD44 FITC (BD Biosciences, Clone IM7; Cat. No. 553133), anti-CD49b PE (BioLegend, Clone DX5; Cat. No. 108908) and anti-CD19 PE/Cyanine7 (BioLegend, Clone 6D5; Cat. No. 115520)] or myeloid immune cells panel [anti-CD45 BUV395 (BD Biosciences, Clone 30-F11; Cat. No. 564279), anti-CD11b PerCP-Cy5.5 (BD Biosciences, Clone M1/70; Cat. No. 550993), anti-GR1 APC (BD Biosciences, Clone RB6-8C5; Cat. No. 553129), anti-CD11c PE (BioLegend, Clone N418; Cat. No. 117308), anti-CD80 BV421 (Biolegend, Clone 16-10A1; Cat. No. 104725), anti-F4/80 PE/Cyanine7 (BioLegend, Clone BM8; Cat. No. 123114), and anti-CD206 BV650 (BioLegend, Clone C086C2; Cat. No. 141723)] on ice for 20 minutes in the dark. Samples were washed with FACS buffer, then fixed with 400 μL of 1% paraformaldehyde (Fisher; Cat. No. 50-980-487) and protected from light. Stained samples were read on a Symphony FLOW cytometer (BD Biosciences) and analyzed using FCS Express software (DeNovo Software, Pasadena, CA).

Intracellular flow cytometry

The cells were then harvested and underwent the same surface staining process as described for lymphoid panel above with the following antibodies: anti-CD3 APC, anti-CD45 BUV395, anti-CD4 BB700, and anti-CD8 BV421. Following extracellular staining, cells were resuspended in fixation buffer (Invitrogen, Cat. No. 00-8222-49) for 20 minutes in the dark, before adding permeabilization buffer (Invitrogen, Cat. No. 00-8333-56). The samples were then stained with anti-T-bet AF594 (Biolegend, clone 4B10: Cat. No. 644834) and incubated for 30 minutes. Following a couple of washes in permeabilization buffer, cells were resuspended in 300 μL PBS for FLOW analysis on the Symphony A5 FLOW cytometer (BD Biosciences) and analyzed using FCS Express software (DeNovo Software, Pasadena, CA).

NanoString sequencing

Four panels purchased from NanoString Technologies were used in this project: PanCancer IO 360™ (Cat. No. LBL-10545-01), Metabolic Pathways (Cat. No. LBL-10726-01), Immunology (Cat. No. LBL-C0268-02), and Myeloid Innate Immunity Panel (Cat. No. LBL-10398-02). NanoString raw data QC was done using nSolver4.0™ software (NanoString Technologies) with default parameters and principal component analysis (PCA). Outlier samples were removed before further analysis. Data were normalized using the nSolver4.0 advanced model, which automates the house-keeping gene selections. Differential gene expression analysis was done using the *limma*[2] package.[82]

HER2 DC1 migration experiment

CellTrace Violet (Invitrogen, Carlsbad, CA; Cat. No. C34557) was used to label HER2 DC1 cells following the manufacturer's protocol, and labeled cells were then injected intratumorally in 12 female BALB/c mice bearing bilateral TUBO tumors with or without combination therapy, six mice for both groups. CellTrace Violet-labeled HER2 DC1 cells were injected into the left flank tumor, and the distant tumor was left untreated. Treated tumors, untreated distant tumors, and tumor-draining lymph nodes were collected after 24 and 48 hours, 3 mice per group and per timepoint. Single cell suspensions were prepared and stained for DCs migration panel [(Live/Dead Zombie near IR (Biolegend, San Diego, CA; Cat. No. 423106), anti-CD45 FITC (Fisher, Clone 30-F11; Cat. No. 11-0451-82), and anti-CD11c BV785 (BioLegend, Clone N418; Cat. No. 117336)] and analyzed by flow cytometry on an LSRII flow cytometer (BD Biosciences) and analyzed using FCS express (*De Novo* Software).

QUANTIFICATION AND STATISTICAL ANALYSIS

Quantitative image analysis

Multi-layer TIFF images were exported from InForm (AKOYA Biosciences, Marlborough, MA) and loaded into HALO Image Analysis Platform version 3.6.4134 (Indica Labs, Albuquerque, New Mexico) for quantitative image analysis. The tissue was segmented into individual cells using the DAPI marker, which stains cell nuclei. For each marker, a positivity threshold is determined within the nucleus or cytoplasm, based on visual intensity, per marker. After setting a positive fluorescent threshold for each staining marker, the image set was analyzed using the algorithm created. The generated data includes positive cell counts for each fluorescent marker in the cytoplasm or nucleus and the percentage of cells positive for the marker.

Sema4D expression in human breast cancer patients

The Cancer Genome Atlas (TCGA) RNA sequencing (RNA-seq) expression data (FPKM) for *SEMA4D* in breast cancer were downloaded from the Genomic Data Commons Data Portal (GDC; https://portal.gdc.cancer.gov, RRID:SCR_014514) and analyzed as described in.[9]

NanoString sequencing data analysis

Differential expression analyses were performed on four different panels: PanCancer Pathway (750 genes), Immunology (547 genes), Metabolic Pathways (748), and Myeloid Innate immunity (734 genes) between treatment groups and control samples filtered using the following cutoffs: 2-fold change, and p-value <0.05. Differentially expressed genes from all the panels were combined and pruned to discard the overlapped genes. Venn diagrams were generated through VENNY 2.1 (https://bioinfogp.cnb.csic.es/tools/venny/index.html). Pathway enrichment of differentially expressed genes was performed with MetaCore (Clarivate Analytics, Philadelphia, PA).

Statistical analysis

All data were displayed as the mean ± standard error of the mean (SEM) or standard deviation (SD). Statistical analysis was performed with GraphPad Prism 9.0 or later. Mean differences were compared for various experimental groups using a Fisher exact test, t-test, Mann-Whitney test, one-way analysis of variance (ANOVA) with Tukey's multiple comparisons post hoc test, Kruskal-Wallis test, and two-way ANOVA. Histogram distribution was compared using Kolmogorov-Smirnov test. Survival proportions were analyzed using Mantel-Cox Log-Rank testing. The respective test used for each experiment is explicitly described in the figure legends. Statistical significance was determined by p-values calculated at $p<0.05$.

Cell Reports, Volume *45*

Supplemental information

Potentiating dendritic cell immunotherapy by interrupting the Semaphorin 4D-induced immune-suppressive barrier

Saurabh K. Garg, Colin Snyder, Ganesan Ramamoorthi, Krithika N. Kodumudi, Elizabeth E. Evans, Vincent Lok, Holm Bussler, Jonathan V. Nguyen, Jiqiang Yao, Amrita Basu, Namrata Gautam, Julio A. Vazquez Martinez, Darwin C. Chang, Amy L. Aldrich, Doris Wiener, Paulo C. Rodriguez, Maurice Zauderer, Gary K. Koski, and Brian J. Czerniecki

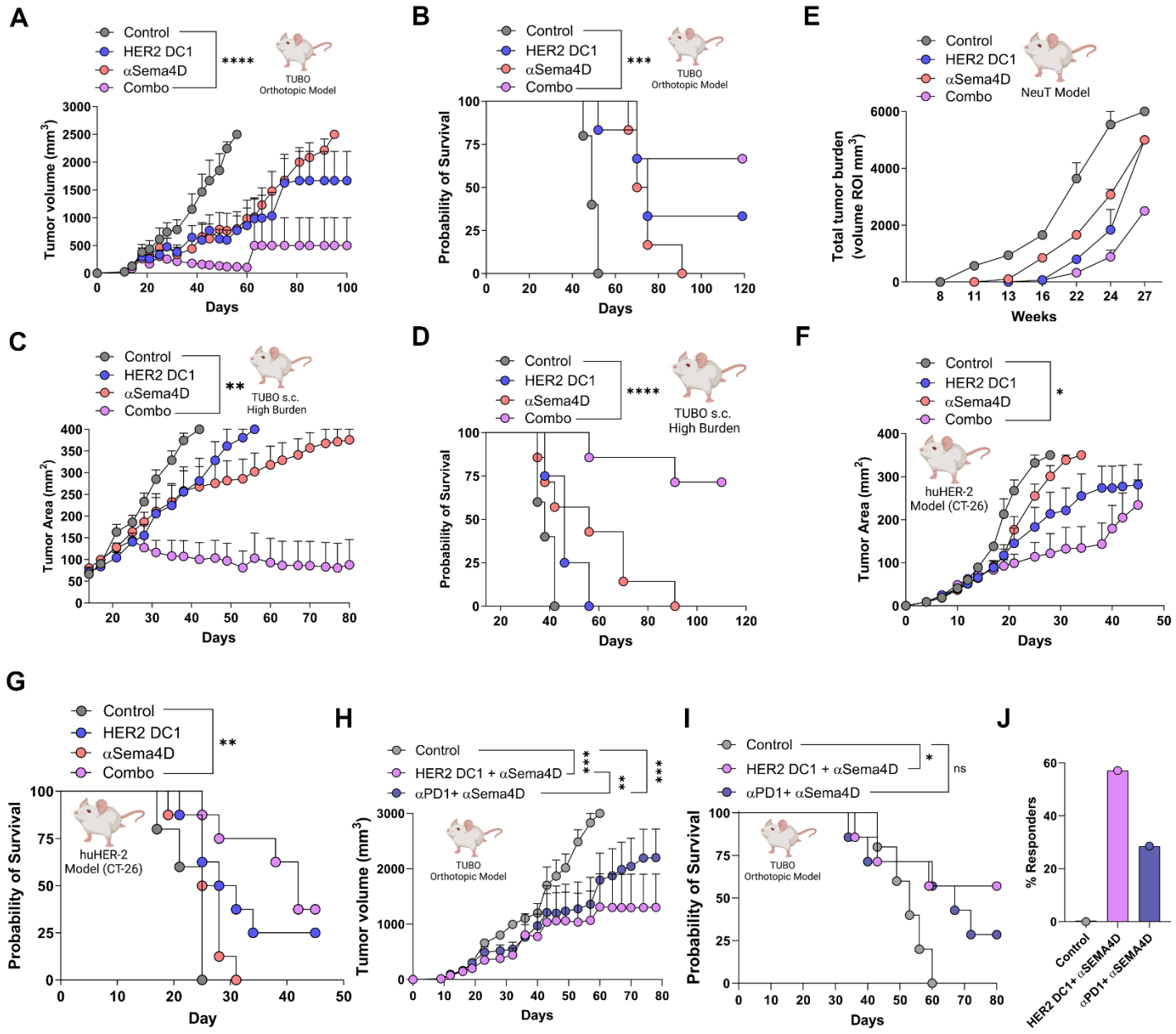

Figure S1. IT delivery of HER2 DC1 in combination with αSema4D demonstrates robust efficacy in multiple HER2^{pos} BC models.

(A-B) Efficacy of HER2 DC1-αSema4D in the orthotopic model. BALB/c mice were inoculated with TUBO cells in a mammary fat pad (MFP). **(A)** Tumor growth was monitored with a caliper two times a week (n=8 mice per group). Data are represented as mean +/- SEM. Statistics using one-way ANOVA. **(B)** Kaplan-Meier curve showing a significant effect of combination therapy on survival. Statistics using the long-rank test. **(C-D)** Effect of combination therapy in high tumor burden model (larger TUBO model). Treatment was started when the tumor size reached 75-100mm^2. **(C)** Tumor growth was monitored with a caliper two times a week (n=7 mice per group). Data are represented as mean +/- SEM. Statistics using one-way ANOVA. **(D)** Survival curves of the larger TUBO tumor burden model received various treatments as indicated. Statistics using the long-rank test. **(E)** The efficacy of HER2 DC1 with αSema4D was also tested in the spontaneous mammary carcinoma

model (NeuT-BALB/c). Tumor growth was monitored via MRI every 2-3 weeks (n=5 mice per group). Data are represented as mean +/- SEM. Statistics using one-way ANOVA. **(F-G)** The efficacy of HER2 DC1 and αSema4D combination therapy in human HER2+ tumor model (CT-26). **(F)** Tumor growth curves of mice bearing the CT-26 (hHER2) tumor model. After tumor establishment, mice were treated with HER2 DC1 alone or αSema4D IgG or in combination as described (n=8 mice per group). Data are represented as mean +/- SEM. Statistics using one-way ANOVA. **(G)** Kaplan-Meier curve of the CT-26 model. Statistics using the long-rank test. **(H-J)** Effect of integrating SEMA4D blockade with checkpoint blockade and its comparison to cDC1-αSema4D therapy in orthotopic TUBO model. **(H)** Tumor growth was monitored with a caliper two times a week (n=7 mice per group). Data are represented as mean +/- SEM. Statistics using one-way ANOVA. **(I)** Kaplan-Meier curve showing a significant effect of combination therapy on survival. Statistics using the long-rank test. **(J)** Bar plot depicting the response rate of various treatments based on the eradication of the implanted tumor by day 80 in the mammary fat pad orthotopic model.

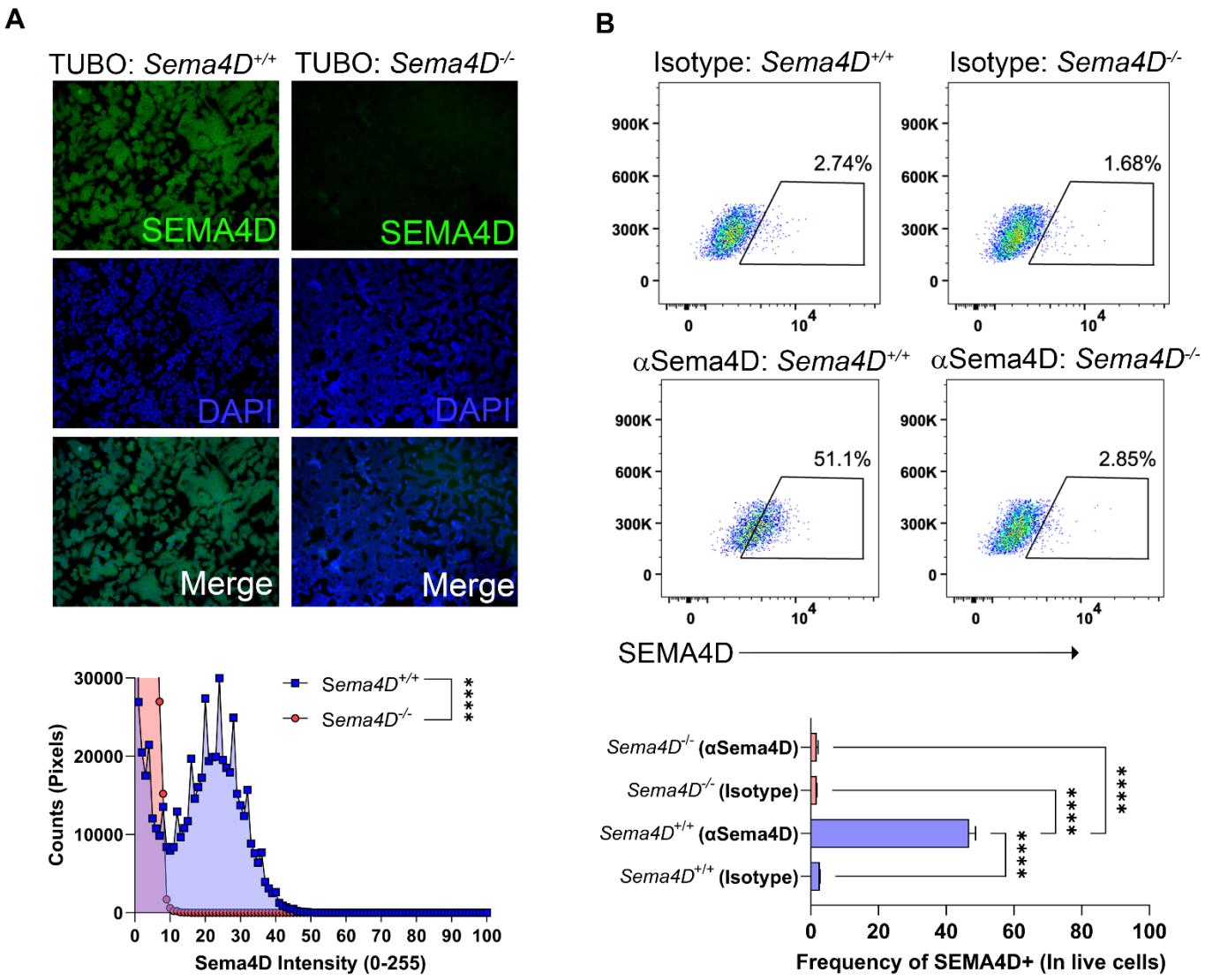

Figure S2. QC of SEMA4D CRISPR knockout of TUBO cells.
(A) Immunofluorescence analysis of WT and SEMA4D-deficient TUBO. IF images were quantified for pixel intensity in the SEMA4D channel using ImageJ. ****P < 0.0001 by Kolmogorov-Smirnov Test. **(B)** Measurement of surface SEMA4D expression from WT and SEMA4D-deficient TUBO by flow cytometry. Data are represented as mean +/- SEM. ****P < 0.0001 by one-way ANOVA.

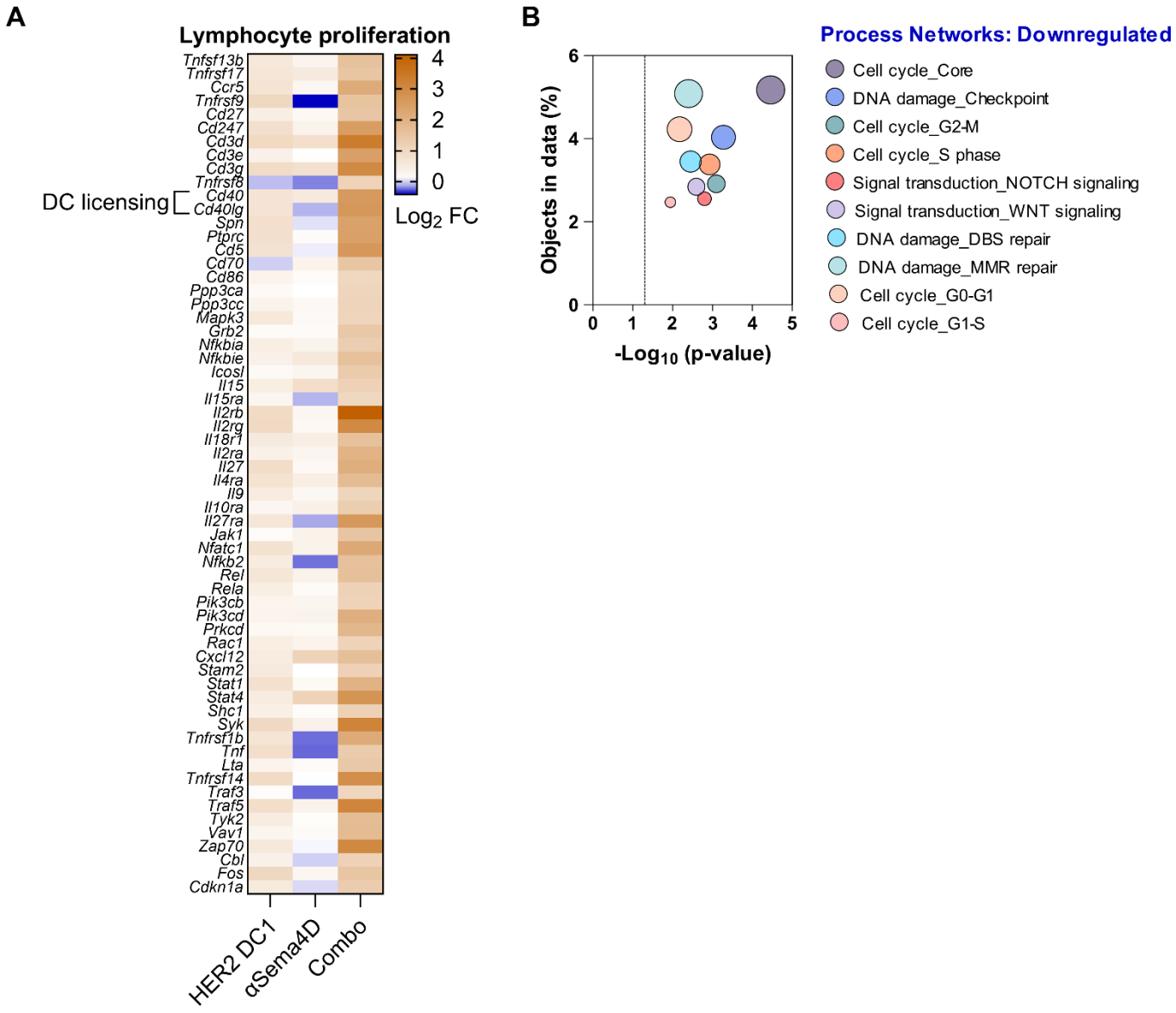

Figure S3. Analysis of nanostring data following HER2 DC1- αSema4D therapy.
(A) Pathway enrichment analysis of expression data of HER2 DC1, αSema4D, and combination treatments showed elevated expression of genes involved in lymphocyte proliferation in the combination group compared to controls. **(B)** Showing enrichment of top 10 process networks of down-regulated datasets following combination therapy in comparison to control. The dotted line is the adjusted P value = 0.05.

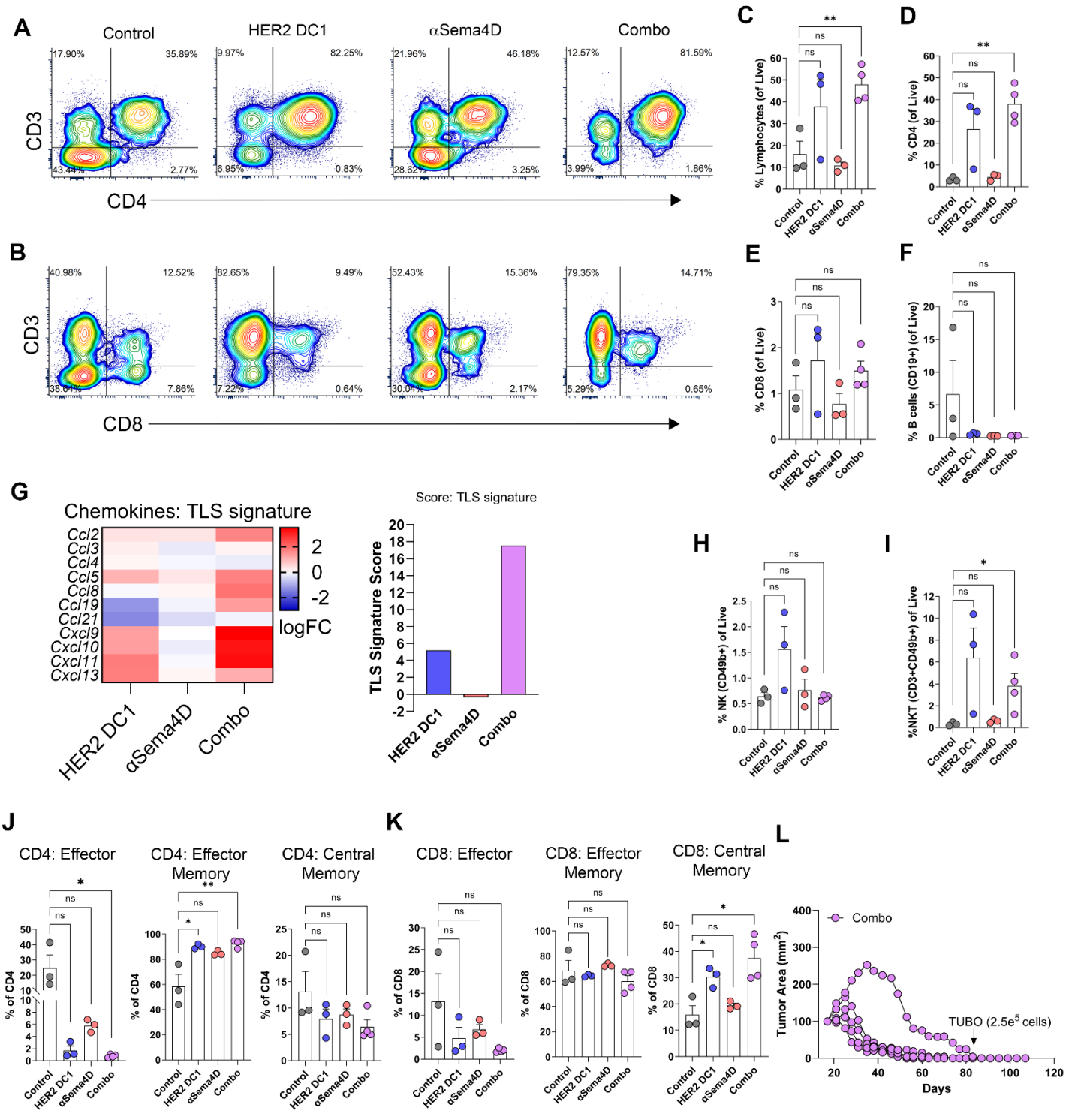

Figure S4. Combination therapy boosts the effector memory phenotype of T cells.
(A-B) Flow cytometry analysis shows $CD4^+$ and $CD8^+$ T cell frequencies in the tumors treated with monotherapies and combination therapy. **(C-F)** Immune profiling of tumor-infiltrating lymphocytes by flow cytometry. Data are represented as mean +/- SEM. Non-significant, $^{**}P < 0.01$ by t-test. **(C)** Fraction of

lymphocytes of all cells. **(D)** Fraction of $CD4^+$ cells of all viable cells. **(E)** Fraction of $CD8^+$ cells of all viable cells. **(F)** Fraction of $CD19^+$ B cells of all viable cells. **(G)** Pathway enrichment analysis of HER2 DC1, Sema4D, and combination treatment expression data showed elevated expression of genes related to chemokines implicated in TLS formation, with corresponding scores shown on the right. **(H-I)** Immune profiling of tumor-infiltrating innate effectors by flow cytometry. Data are represented as mean +/- SEM. Non-significant, *$P < 0.05$ by t-test. **(H)** Fraction of $CD49b^+$ NK cells of all viable cells. **(I)** Fraction of CD3 $CD49b^+$ NKT cells of all viable cells. **(J)** Memory phenotype of $CD4^+$ T cells. Fraction of CD4 effectors ($CD44^-$ $CD62L^-$) of cells. Fraction of CD4 effector memory ($CD44^+$ $CD62L^-$) cells. Fraction of CD4 central memory ($CD44^+$ $CD62L^+$) cells. Data are represented as mean +/- SEM. Non-significant, *$P < 0.05$, **$P < 0.01$ by t-test. **(K)** Memory phenotype of $CD8^+$ T cells. Fraction of CD8 effectors ($CD44^-$ $CD62L^-$) cells. Fraction of CD8 effector memory ($CD44^+$ $CD62L^-$) cells. Fraction of CD8 central memory ($CD44^+$ $CD62L^+$) cells. Data are represented as mean +/- SEM. Non-significant, *$P < 0.05$ by t-test. **(L)** Combination therapy elicits long-lasting immunity. Tumor growth curve of responder mice from the high tumor burden model. Mice were rechallenged with TUBO cells, and tumor growth was monitored with a caliper two times a week.

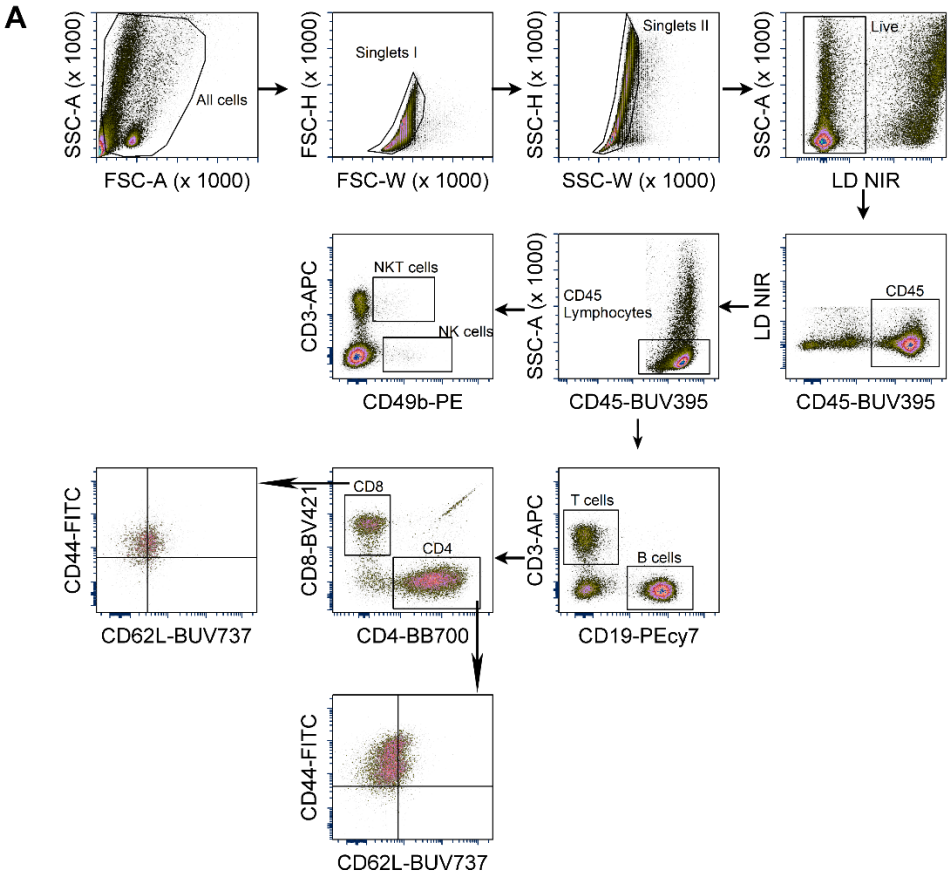

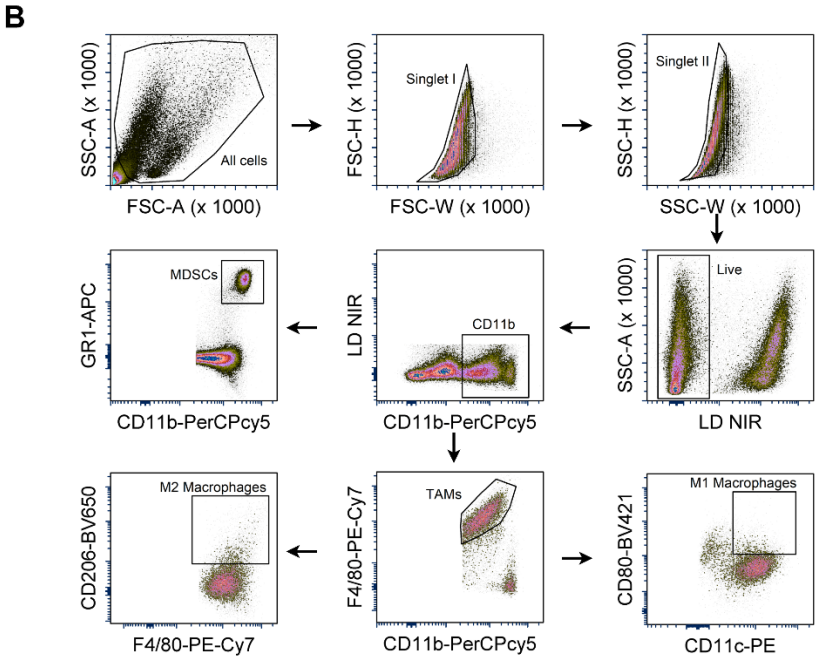

Figure S5. Gating strategy to characterize various immune cell populations from TME.

(A) Gating strategy to characterize the effector phenotype of the lymphoid immune population from the tumors treated with different therapies. **(B)** Gating strategy to characterize suppressor phenotype of the myeloid immune population from the tumors treated with different therapies. Flow plots are generated in FCS Express 7.0 (DeNovo Systems).

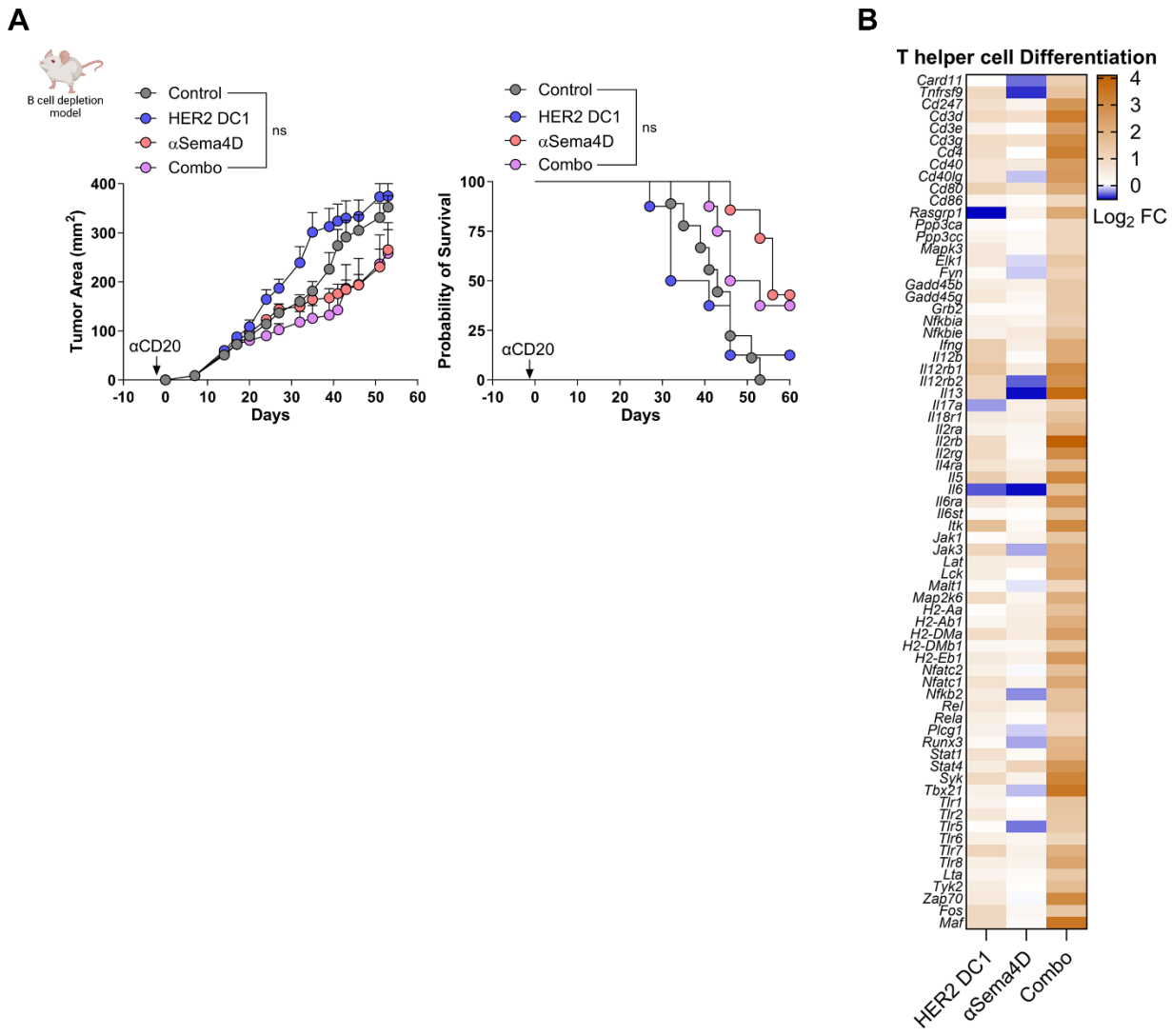

Figure S6. B-cell function is important for the successful effect of combination therapy.
(A) Tumor growth curves and survival curves of the B cell depletion model. BALB/c mice were injected with αCD20 antibody one day prior to TUBO inoculation. After TUBO tumor establishment, mice received different therapies as indicated (n=6 mice per group). Tumor growth in the depletion model was monitored with a caliper two times a week. Data are represented as mean +/- SEM. Statistics using one-way ANOVA. Kaplan-Meier curve of the B cell depletion model. Statistics using the log-rank test. **(B)** Pathway enrichment analysis of expression data of HER2 DC1, αSema4D, and HER2 DC1-αSema4D treatments showed elevated gene expression in T helper cell differentiation in the combination group compared to controls.

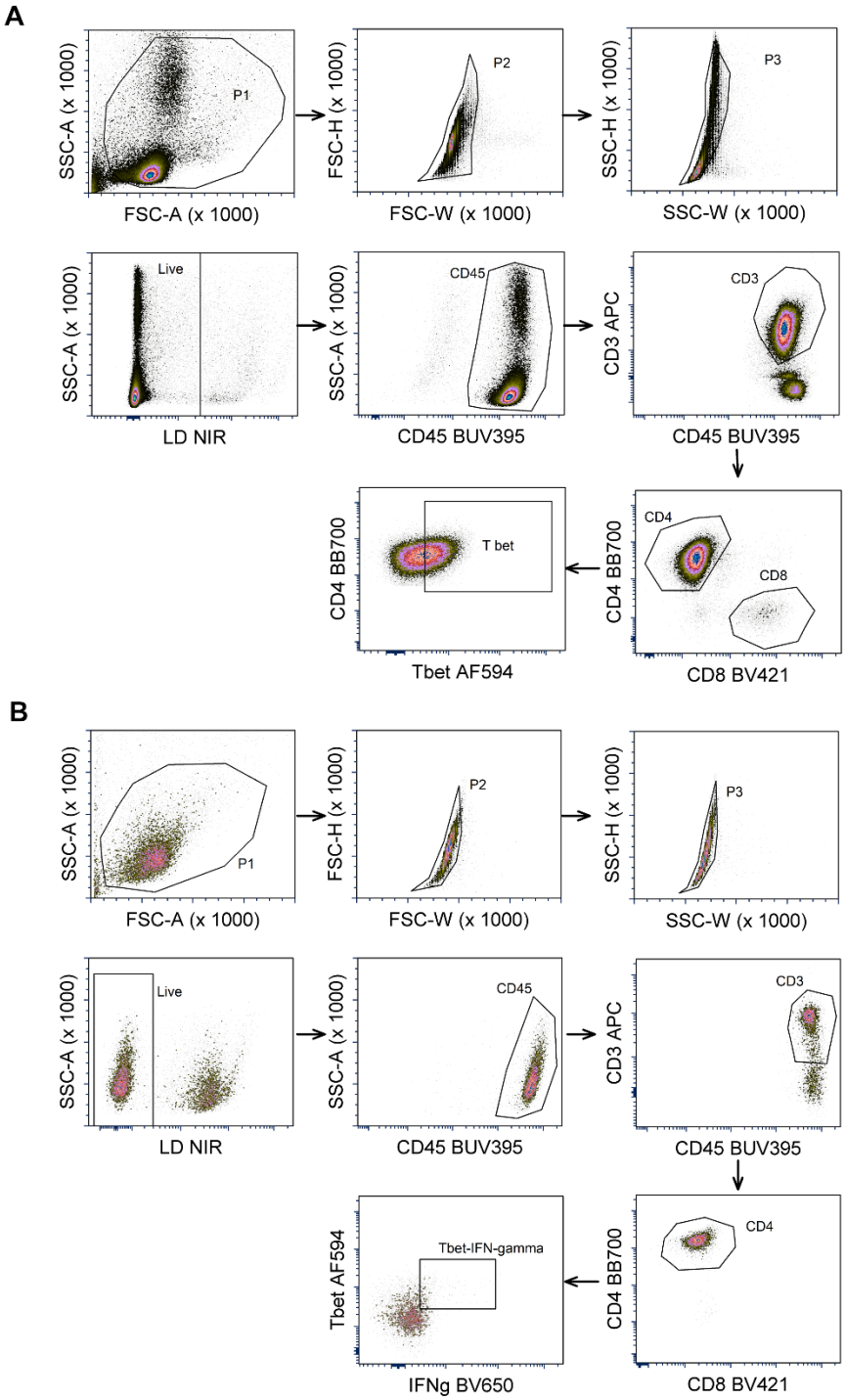

Figure S7. Flow gating to analyze T-bet and IFN-γ in CD4$^+$ T cells.
(A) Gating strategy to measure the frequency of T-bet-expressing CD4$^+$ T cells from mice treated with different therapies. **(B)** Gating strategy to measure frequency of T-bet-IFN-γ double-positive CD4$^+$ T cells from DC1-T cell co-culture experiment. Flow plots are generated in FCS Express 7.0 (DeNovo Systems).

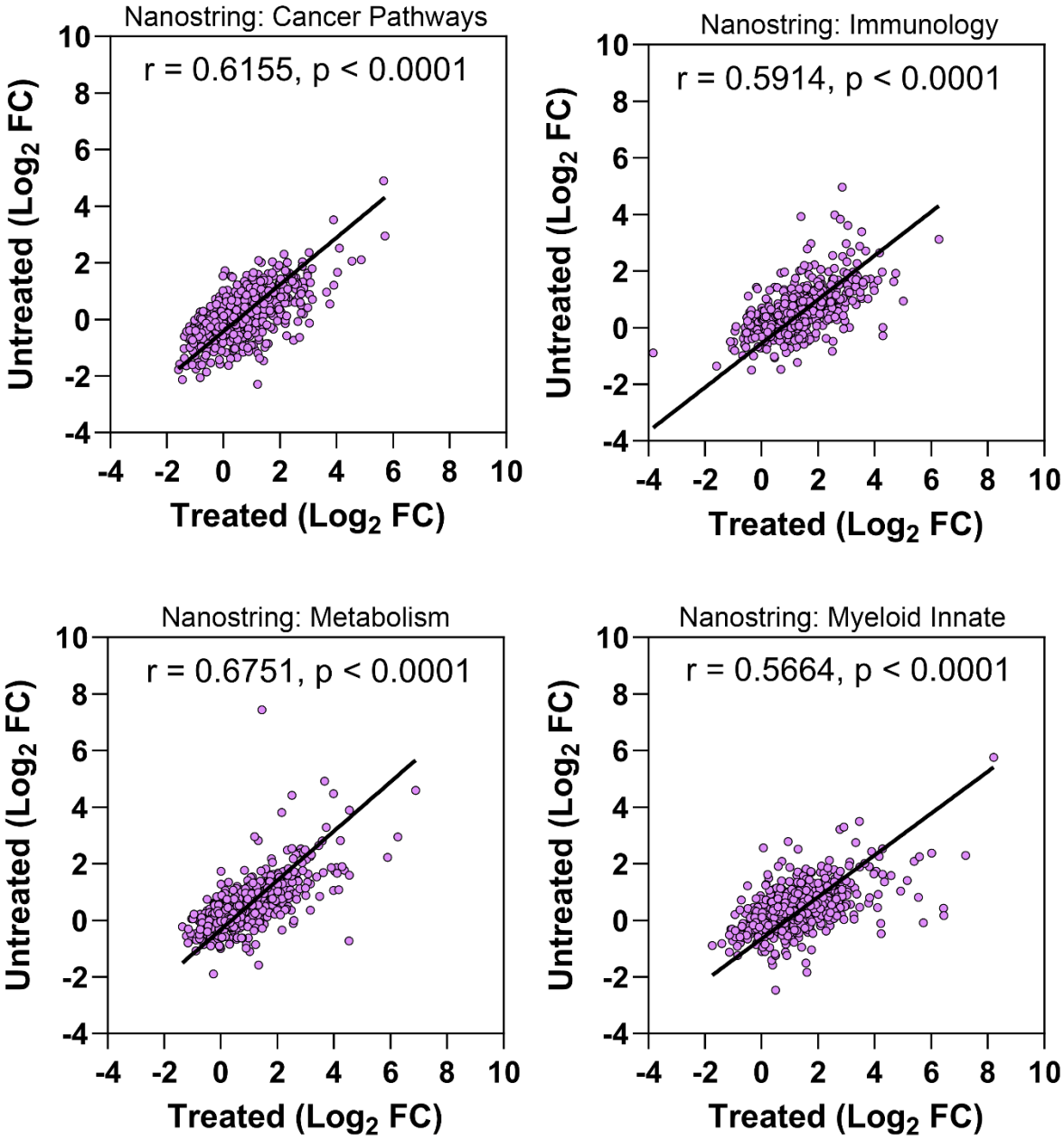

Figure S8. Overlapping molecular signature of response between primary and abscopal effect.
Scatter plots of gene expression changes of four Nanostring panels of treated and untreated tumor flanks of HER2 DC1-αSema4D treated mice show a strong correlation between the two datasets. Statistics using Pearson correlation.

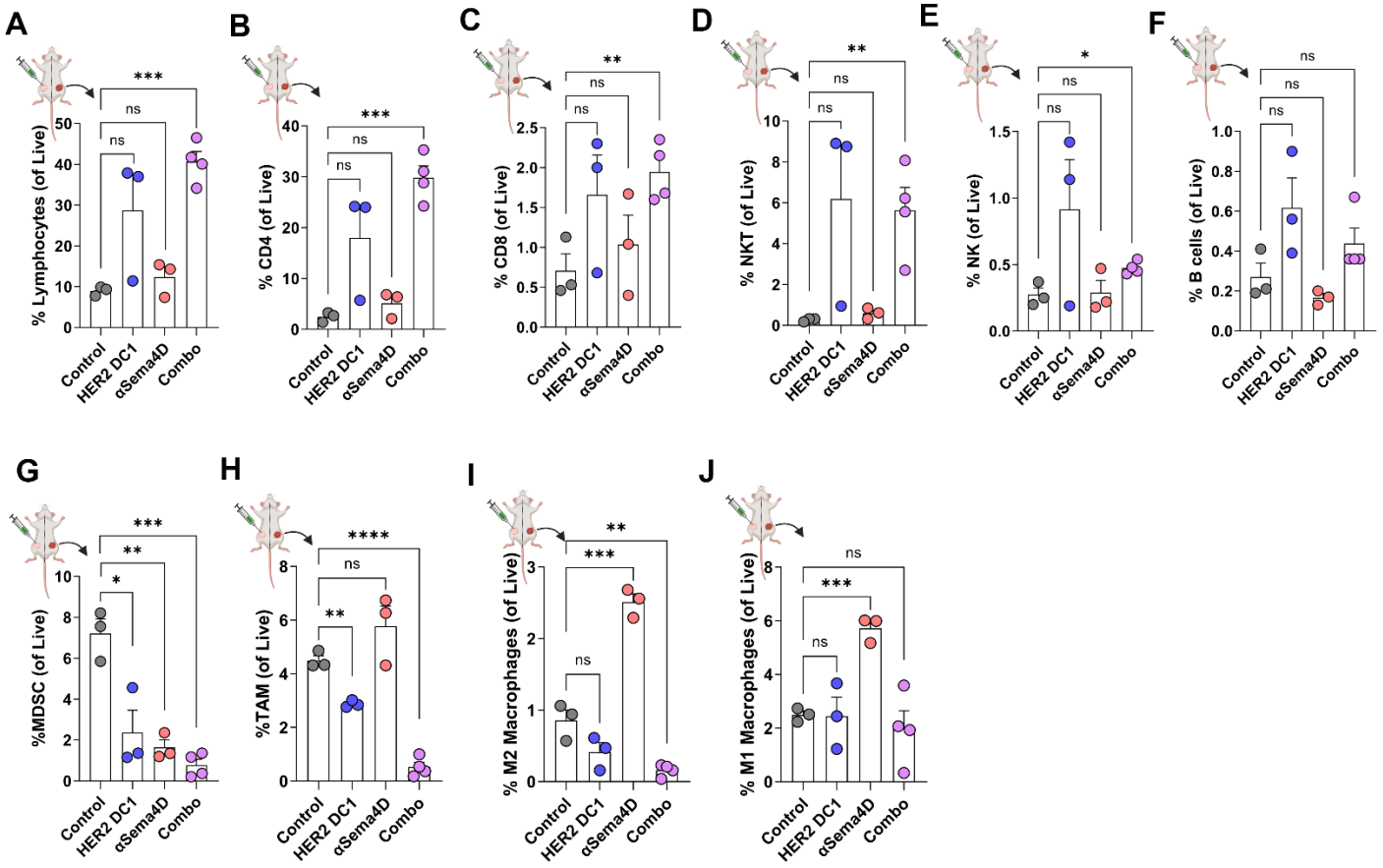

Figure S9. Immune cell phenotype of the untreated tumor in the bilateral tumor model.
(A-F) Immune profiling of the effector phenotype of tumor-infiltrating lymphocytes by flow cytometry analysis of the untreated tumor of the bilateral model. Data are represented as mean +/- SEM. Non-significant, *P < 0.05, **P < 0.01, ***P < 0.001, ****P < 0.0001 by t-test. **(A)** Fraction of lymphocytes of all viable cells. **(B)** Fraction of $CD4^+$ cells of all viable cells. **(C)** Fraction of $CD8^+$ cells of all viable cells. **(D)** Fraction of NKT cells of all viable cells. **(E)** Fraction of NK cells of all viable cells.
(F) Fraction of B cells of all viable cells. **(G-J)** Immune profiling of the myeloid phenotype of tumor-infiltrating lymphocytes by flow cytometry analysis of the untreated tumor of the bilateral model. Data are represented as mean +/- SEM. Non-significant, *P < 0.05, **P < 0.01, ***P < 0.001, ****P < 0.0001 by t-test. **(G)** Fraction of Myeloid-derived suppressor cells (MDSC) of all viable cells. **(H** Fraction of tumor-associated macrophages (TAM) of all viable cells. **(I)** Fraction of M2 macrophages of all viable cells. **(J)** Fraction of M1 macrophages of all viable cells.

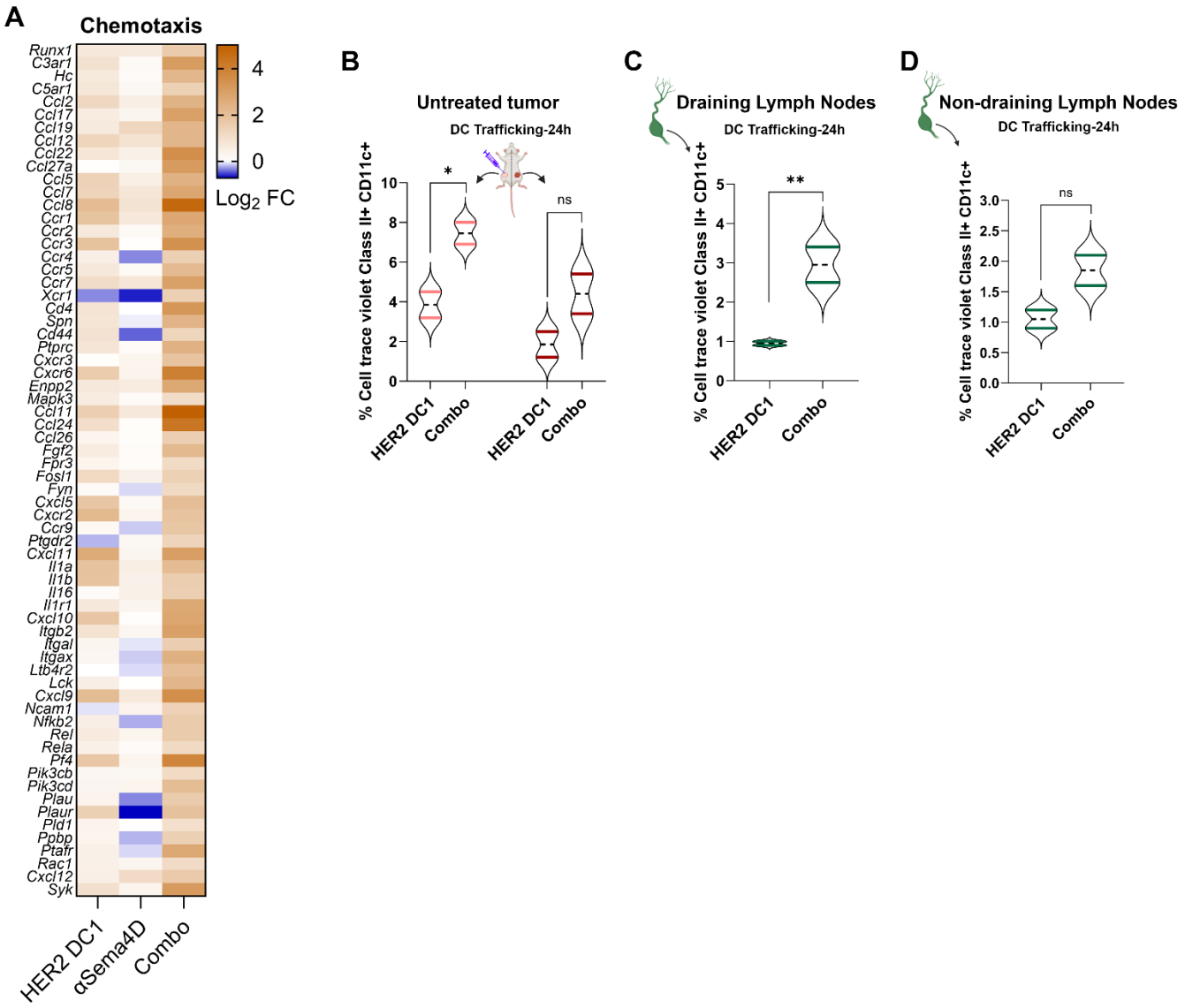

Figure S10. DC trafficking following HER2 DC1-αSema4D therapy.
(A) Pathway enrichment analysis of expression data of HER2 DC1, αSema4D, and HER2 DC1-αSema4D treatments showed elevated gene expression in chemotaxis in the HER2 DC1 alone and combination group compared to controls. **(B)** Post 24 hours labeled cDC1 trafficking to the distal tumor in the bilateral TUBO model. Data are represented as mean +/- SEM. Non-significant, *P < 0.05 by two-way ANOVA. **(C)** Post 24 hours labeled cDC1 trafficking to DLN. Data are represented as mean +/- SEM. **P < 0.01 by two-way ANOVA. **(D)** Post 24 hours labeled cDC1 trafficking to non-draining lymph node (nDLN). Data are represented as mean +/- SEM. Non-significant by two-way ANOVA.

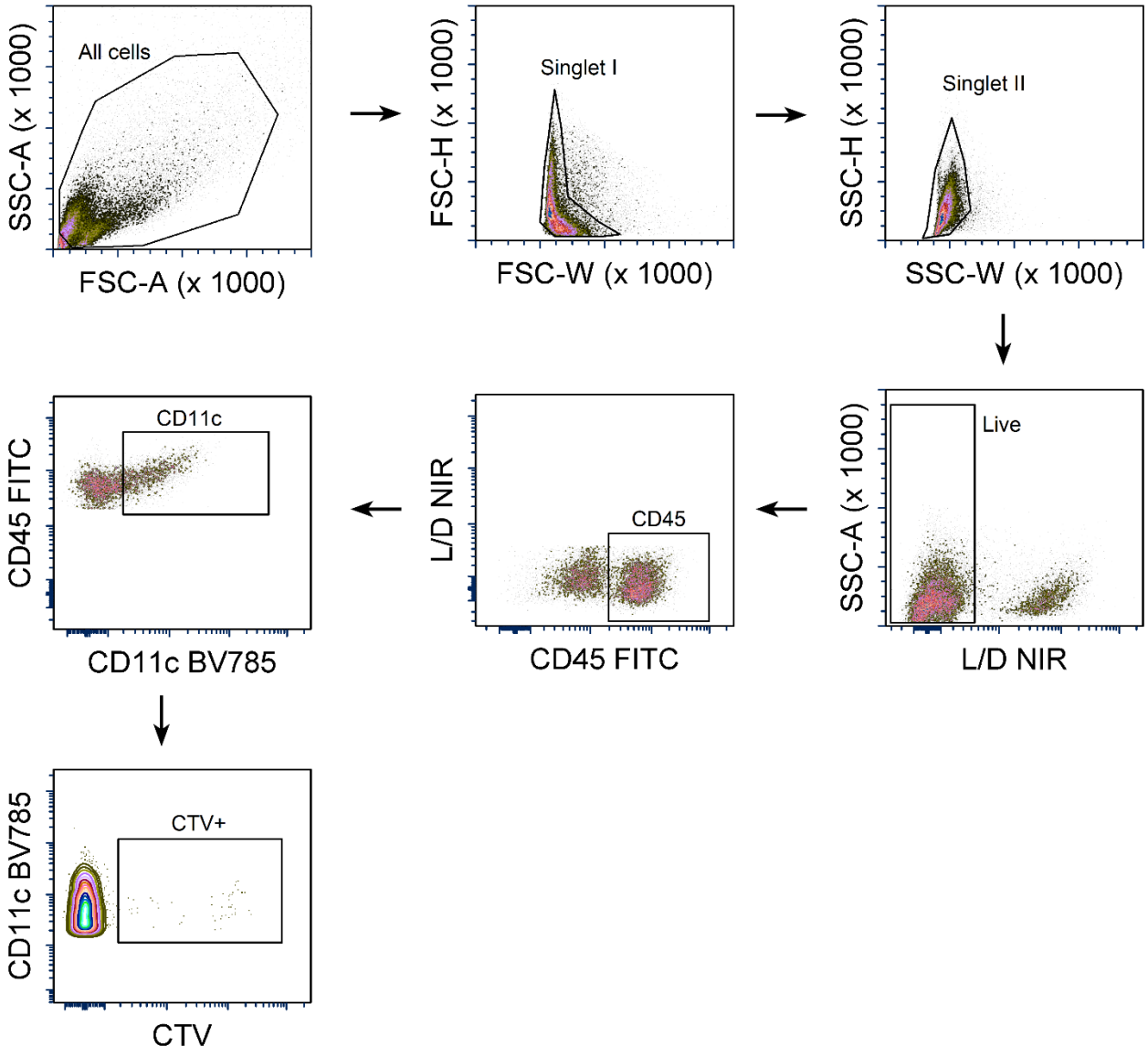

Figure S11. Gating strategy to follow the DC migration.
Strategy to follow CellTrace violet-labeled CD11c-positive cDC1 population from the untreated tumors of mice treated with different therapies. Flow plots are generated in FCS Express 7.0 (DeNovo Systems).

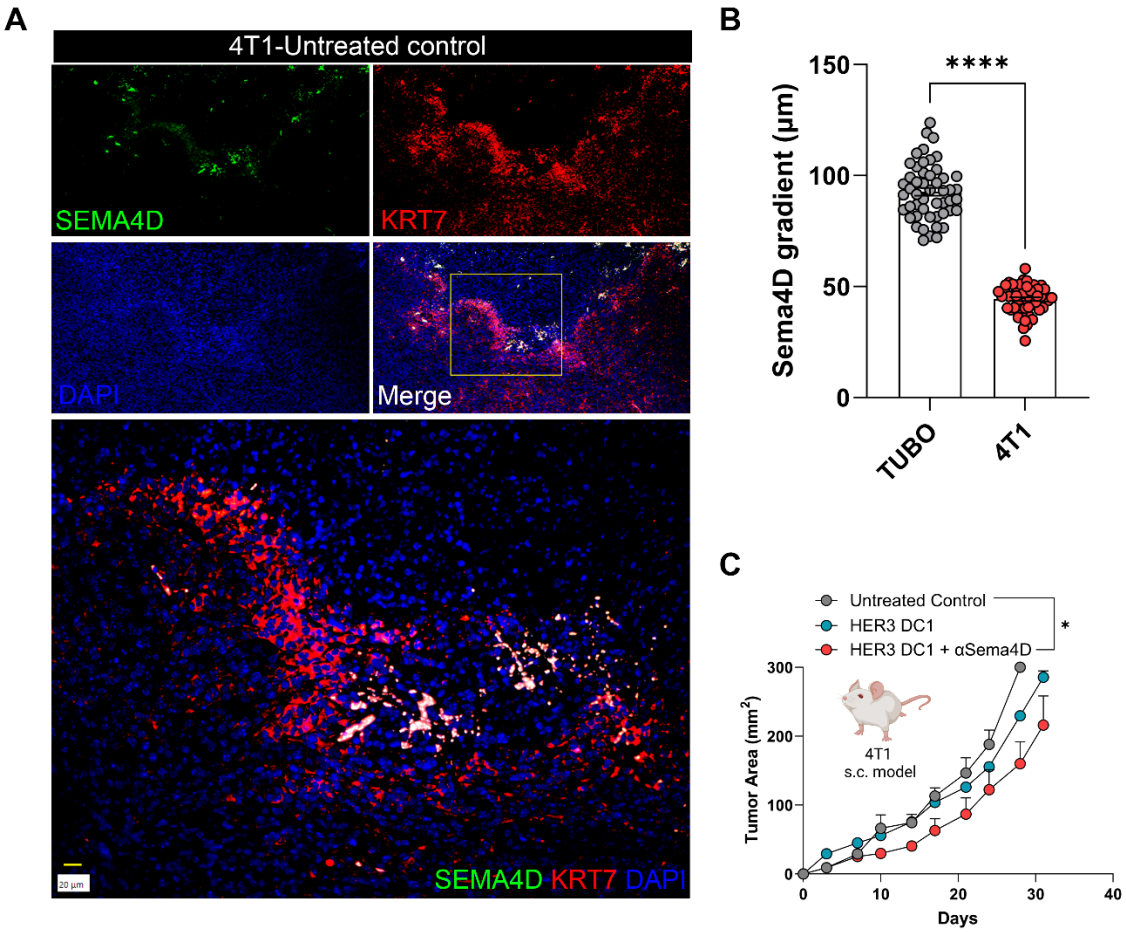

Figure S12. Expression analysis of SEMA4D from the 4T1 TNBC model.
(A) IF imaging from untreated 4T1 tumors shows SEMA4D expression on the invasive margins of the tumor. The scale bar on high-magnification images is 20µm. **(B)** The SEMA4D gradient was compared to TUBO tumors by x-y measurements as shown in Figure 1G. Data are represented as mean +/- SEM. ****P < 0.0001 by Mann-Whitney test. **(C)** Tumor growth curve showing the combination of IT tumor-directed cDC1 with SEMA4D blocking. BALB/c mice were inoculated with $4e^5$ 4T1 cells subcutaneously. Tumor growth was monitored using a caliper twice a week (n=6 mice per group). Data are represented as mean +/- SEM. Statistics using one-way ANOVA.